PERGAMON

International Journal of Solids and Structures 39 (2002) 6211–6240

INTERNATIONAL JOURNAL OF SOLIDS and STRUCTURES

www.elsevier.com/locate/ijsolstr

A lumped stress method for plane elastic problems and the discrete-continuum approximation

Fernando Fraternali *, Maurizio Angelillo, Antonio Fortunato

Department of Civil Engineering, University of Salerno, 84084 Fisciano (SA), Italy

Received 15 February 2001; received in revised form 8 August 2002

Abstract

This paper proposes a rational method to approximate a plane elastic body through a latticed structure composed of truss elements. The method is based on the introduction of a relaxed stress energy that allows an extension of the original problem to a larger space of admissible stress fields, including stresses concentrated along lines. Use is made of polyhedral approximations of the Airy stress function. The truss analogy is employed to obtain a displacement formulation. The paper includes several numerical applications of the method to sample problems, a numerical convergence study and comparisons with exact solutions and standard finite element approximations.

Keywords: Plane elasticity; Anisotropy; Airy's stress function; External mixed methods; Truss analogy

1. Introduction

This work presents a new numerical method for plane elastic problems (*lumped stress method* or LSM), which can be thought of as a rational technique for modeling a plane body through a network of truss elements. Fundamentally this approach was inspired by the *lumped strain method* for isotropic Kirchhoff plates of Davini and Pitacco (1998, 2000), which is extended here to treat Airy's formulation of anisotropic plane elasticity.

The approximation of a continuum medium with an "equivalent" truss structure is often sought in technical applications. For example, it is common practice for structural engineers to employ truss analogies for modeling reinforced concrete and masonry members, as the Mörsch-mechanism of shear resistance in r.c. beams, funicular polygons, network models, and the recent strut-and-tie methods.

This type of modeling is frequently motivated by one of the following: coupling of 2D or 3D elements (like panels, walls, deep beams, etc.) with effective networks of 1D elements (frames, trusses, etc.); use of stress resultant and moments in technical codes; and a significantly simplified treatment of plasticity and no-tension constraints.

* Corresponding author. Tel.: +39-089-964083; fax: +39-089-964045.
E-mail address: f.fraternali@unisa.it (F. Fraternali).

0020-7683/02/$ - see front matter
PII: S0020-7683(02)00472-9

Several procedures using equivalence methods or minimization of suitable objective functions are available in the literature (see, e.g., Absi, 1978; Papadopoulos, 1984; Schlaich and Schäfer, 1991; Biondini et al., 1999; O'Dwyer, 1999). A serious concern is the choice of a correct network in the case of complicated loadings or member geometries. In most cases, bar elements must be placed along the principal directions of stress and the convergence of the numerical approximations, if available, is valid for a particular load condition and/or for particular material properties. Nevertheless, in recent years, the advances in interactive computer graphics have considerably increased the utility of methods like strut-and-tie (Alshegeir and Ramirez, 1992; Mish, 1994), that are beginning to be considered by several technical codes (as ACI and AASHTO) as useful tools in the design of structural concrete members.

Opposing approaches have also been proposed and widely used in the past for coupled shear walls, shear walls interacting with frames, multi-beam bridges and other systems (Rosman-Beck, Massonet-Bareš and similar models). Recently, the homogenization theory, evolutionary and genetic algorithms have been used to design an optimal truss over a given reference domain (see, e.g., Hajela and Lee, 1995; Bendsøe and Kikuchi, 1998; Ohsaki, 1998; Moreau, 1998; Bulman et al., 2001).

The LSM views the transition from a continuum to a structure as an extension of the continuous equilibrium problem to a larger space of test functions for the stress field. In fact, the stress "runs" along preferential lines (or surfaces) in a structural network and such singularities are "non-conforming" for the continuous problem, in a sense that give rise to infinite stress energy.

In the LSM, a plane body Ω is discretized through two complementary meshes: a *primal mesh* consisting of a triangulation of Ω; and a *dual mesh* formed by polygons encircling the nodes of the primal mesh. The *skeleton* of the primal mesh is used to approximate the stress field through uniaxial singular stresses, while the dual mesh is used to average such singularities in the neighborhood of each primal node. In this way the final description of the stress field is piecewise constant.

Approximate solutions of the 2D problem are found by minimizing a *relaxed* complementary energy functional $\mathscr{E}_h$, depending on the mesh size h, whose quadratic part (stress energy) is obtained through square integration of the piecewise constant stress.

The result of the approximation is simple from a physical point of view: the body is approximated by a *non-conventional* truss structure $\mathscr{B}_h$, having the same topology as the skeleton of the primal mesh and the complementary energy ($\mathscr{E}_h$) as defined per dual elements (i.e., per nodes) and not per bar elements.

Moving on to examine the case of a 3D body, the proposed methodology can be naturally widened by dividing the body into a collection of tetrahedra (primal mesh) and representing the stress field through stresses concentrated over planes (the facets of the tetrahedra). In this way, the body is approximated by a network of shell elements (*description of a* 3D *body by a collection of* 2D *elements*). A relaxed energy can be defined averaging the singular stresses over polyhedra (dual elements) which surround the vertices of primal elements. Alternatively, one can imagine representing the 3D stress field by linear concentrated stresses, arriving at a modeling of the body through a spatial truss structure (1D *elements*).

The mathematical formulation of the LSM is obtained when the Airy stress function φ is introduced. Indeed, a distribution of balanced singular stresses can be generated from a piecewise linear approximation $\widehat{\varphi}$ of the Airy function, whose graph forms a *polyhedral surface*. Each singular stress corresponds with a fold of this surface; in particular, convex and concave folds generate tensile and compressive stresses, respectively. The piecewise constant approximation of the stress field corresponds with a discrete notion of the *Hessian tensor* of $\widehat{\varphi}$.

The LSM falls within the framework of mixed approximation methods for fourth-order partial differential equations, extensively studied by Glowinski (1973), Ciarlet and Raviart (1974, 1978), and several other authors (see Scholtz, 1978, 1979; Brezzi and Fortin, 1991; Oden and Carey, 1983b; Balasundaram and Bhattacharyya, 1986), mainly referring to the biharmonic equation.

In a recent work (Fraternali, 2001), we have deduced the LSM convergence order in the case of traction problems, accounting for the more general fourth-order problem of anisotropic plane elasticity (Airy's

formulation). This significant result has been deduced on assuming suitable hypotheses on the topology of the mesh, which are not necessary in the biharmonic case (isotropic elasticity).

Here we expand the LSM stress function formulation (SFF) to cover problems with mixed boundary conditions. Furthermore, we employ the truss analogy to come up with a displacement formulation, which is applicable to multiple-connected bodies. Finally, we assess the convergence of the method through numerical experiments, establishing comparisons with analytic solutions and standard finite element approximations. We also discuss some interesting numerical properties of the LSM, and especially its accuracy in predicting the stress field, even with relatively coarse meshes and tricky singular loads. A generalization of the method to treat plastic and/or no-tension materials will be developed in proceeding works.

2. Mathematical setting of the lumped stress method

2.1. Airy's formulation of a traction problem of plane elasticity

Consider the elastic problem of a plane body occupying a bounded and simply connected open region Ω of the two-dimensional Euclidean space. For the sake of simplicity, assume that $\overline{\Omega}$ is a polygonal set and initially suppose that its boundary Γ is completely free of kinematical constraints (*traction problem*).

Let the body be subjected to body forces $\mathbf{b}$ in Ω, surface tractions $\mathbf{p}$ over Γ and to a field $\overline{\mathbf{E}}$ of externally imposed infinitesimal strains (*initial strains*), due e.g., to thermal effects. In particular, assume that a stress field $\mathbf{T}^*$ which is in equilibrium with the load $(\mathbf{b}, \mathbf{p})$ is known, i.e., a $\mathbf{T}^*$ such that its divergence $\operatorname{div}\mathbf{T}^*$ exists in Ω and it results $\operatorname{div}\mathbf{T}^* + \mathbf{b} = \mathbf{0}$ in Ω, $\mathbf{T}^*\hat{\mathbf{n}} = \mathbf{p}$ over Γ, $\hat{\mathbf{n}}$ being the outward unit normal to Γ.

Finally, let $\{0, x_1, x_2\}$ denote a Cartesian coordinate system in the plane of Ω with unit base vectors $\{\hat{\mathbf{e}}_1, \hat{\mathbf{e}}_2\}$, and use the comma followed by an index, say "$(\cdot)_{,\alpha}$", to indicate differentiation with respect to x_1 and x_2. Let also greek indices range over $\{1, 2\}$, and adopt the summation convention over repeated indices.

Upon introducing a class of scalar functions φ on Ω (*Airy's stress functions*, see e.g., Gurtin, 1972) such that

$$\varphi = 0 \quad \text{and} \quad \frac{\partial\varphi}{\partial n} = 0 \text{ on } \Gamma, \tag{1}$$

a generic stress field $\mathbf{T}$, in equilibrium with the load $(\mathbf{b}, \mathbf{p})$, can be expressed as follows

$$\mathbf{T} = \mathbf{T}^* + \mathbf{W}\mathbf{H}\varphi\mathbf{W}^{\mathrm{T}}. \tag{2}$$

Here, $\mathbf{H}\varphi = \varphi_{,\alpha\beta}\hat{\mathbf{e}}_\alpha \otimes \hat{\mathbf{e}}_\beta$ is the *Hessian tensor* associated with φ, and $\mathbf{W}$ is the skew tensor defined as $\mathbf{W} = e_{\alpha\beta}\hat{\mathbf{e}}_\alpha \otimes \hat{\mathbf{e}}_\beta$, $e_{\alpha\beta}$ indicating two-dimensional alternator and $\otimes$ the symbol of tensor product between vectors.

Denote $\mathbf{A}$ the fourth-order compliance tensor of the material with components $A_{\alpha\beta\gamma\delta}$, and $\mathscr{A}$ the transformed compliance tensor of components

$$\mathscr{A}_{\alpha\beta\gamma\delta} = e_{\alpha\mu}e_{\beta\nu}e_{\gamma\rho}e_{\delta\sigma}A_{\mu\nu\rho\sigma}. \tag{3}$$

The solution $\mathbf{T}_0$ of the elastic problem is characterized by the stress function φ_0 which satisfies the compatibility equation

$$(\mathscr{A}_{\alpha\beta\gamma\delta}\varphi_{,\gamma\delta})_{,\alpha\beta} = f \text{ in } \Omega, \tag{4}$$

where

$$f = -e_{\alpha\mu}e_{\beta\nu}(\overline{E}_{\alpha\beta} + A_{\alpha\beta\gamma\delta}T^*_{\gamma\delta})_{,\mu\nu}. \tag{5}$$

In the particular case of an homogeneous isotropic material, Eq. (4) reduces to the biharmonic equation

$$\Delta\Delta\varphi = \tilde{f}, \tag{6}$$

where Δ is the Laplacian operator, and

$$\tilde{f} = -e_{\alpha\gamma}e_{\beta\delta}(E\overline{E}_{\alpha\beta,\gamma\delta} + T^{*}_{\alpha\beta,\gamma\delta}) + v\mathrm{div}\,\mathbf{b}, \tag{7}$$

E and v being the Young's modulus and the Poisson's ratio of the material, respectively.

Now, let $W^{k,p}(\Omega)$ denote the Solobev space of functions with generalized $L^p(\Omega)$ integrable derivatives upto the kth order, set $H^k(\Omega) = W^{k,2}(\Omega)$, and denote $H^{-k}(\Omega)$ the dual of $H^k_0(\Omega) = \{\varphi \in H^k(\Omega)/\varphi = 0 \text{ on } \Gamma\}$ (cf., e.g., Adams, 1975).

Assume that $\overline{\mathbf{E}}$ and $\mathbf{T}^*$ belong to $H^1(\Omega)$, which implies $f \in H^{-1}(\Omega) \subset H^{-2}(\Omega)$, and that the compliance tensor of the material is positive definite.

A variational formulation of the problem defined by the differential equation (4) and the boundary conditions (1) is the following

Find $\varphi_0 \in H^2_0(\Omega)$ such that

$$\mathscr{E}(\varphi_0) = \inf_{\varphi \in H^2_0(\Omega)} \mathscr{E}(\varphi), \tag{8}$$

where

$$\mathscr{E}(\varphi) = \frac{1}{2}\int_{\Omega} \mathbf{H}\varphi \cdot \mathscr{A}[\mathbf{H}\varphi]\,\mathrm{d}a - l(\varphi), \tag{9}$$

$$l(\varphi) = \langle f, \varphi\rangle_{H^{-2},\ H^2_0}, \tag{10}$$

$\langle\cdot,\cdot\rangle_{H^{-2},\ H^2_0}$ denoting the duality pairing between $H^{-2}(\Omega)$ and $H^2_0(\Omega)$.

2.2. Mixed approach

A mixed approach to (4), (1) consists in splitting Eq. (4) into two second-order equations. That is,

$$\left.\begin{array}{l} \psi_{\alpha\beta} = -\varphi_{,\alpha\beta} \\ (\mathscr{A}_{\alpha\beta\gamma\delta}\ \psi_{\gamma\delta})_{,\alpha\beta} = -f \end{array}\right\} \text{ in } \Omega, \tag{11}$$

where $\boldsymbol{\psi} = \psi_{\alpha\beta}\mathbf{e}_\alpha \otimes \mathbf{e}_\beta$ is an intermediate (or *dual*) variable, which coincides with the opposite of $(\mathbf{T} - \mathbf{T}^*)$ under double permutation of indices.

Such an approach is convenient in developing variational approximations of the boundary value problem, since it allows the use of C^0 test functions for φ, while the originary fourth-order equation calls for C^1 test functions. Obviously, a suitable approximation space for the new variable $\boldsymbol{\psi}$ must also be defined. In particular, by using $(C^0)^4$ test functions, one is led to a *conforming* (or *internal*) approximation of the mixed problem. Notice that $\boldsymbol{\psi}$ is a tensor field, while the *primal* variable φ is a scalar field.

We have seen in the previous section that, for isotropic elastic bodies, Eq. (4) reduces to Eq. (6). A mixed formulation of (6) is the following

$$\left.\begin{array}{l} \psi = -\Delta\varphi \\ \Delta\psi = -f \end{array}\right\} \text{ in } \Omega. \tag{12}$$

Thus, in the isotropic case, both the primary and the dual variable are scalar fields. This point marks an essential difference between mixed approaches to biharmonic and more general fourth-order problems. A similar circumstance arises in the context of the equilibrium problem of elastic Kirchhoff plates (isotropic and anisotropic behavior).

The LSM presented in Section 2.3 extends to problem (11) the mixed method proposed by Davini and Pitacco (1998, 2000) for problem (12). We shall see that the adopted choice of the approximation spaces allows us to eliminate the dual variable from the discrete scheme, thus reducing it to an unconstrained minimization problem.

Remark. External mixed approximations to biharmonic problems were formerly studied by Glowinski (1973), who proved their convergence using direct arguments. Successively, several other authors, and particularly Ciarlet and Raviart (1974, 1978), studied mixed numerical approaches to the biharmonic equation using a systematic theory, coming to detailed error estimates. They examined approximations with piecewise polynomials of order $k \geqslant 2$, for both the primal and the dual variable, over regular triangular meshes. Scholtz (1978, 1979) deduced similar results for piecewise linear polynomials. A generalization of the mixed method by Ciarlet and Raviart can be found in Balasundaram and Bhattacharyya (1986). More recently, Davini and Pitacco (1998, 2000) have resumed Glowinski's method in detail, assuming piecewise linear approximations for the primal variable (φ in our notation) and piecewise constant approximations for the dual variable (ψ).

2.3. The lumped stress method

A variational formulation of the mixed problem (1) and (11) is the following
Find $(\varphi_0, \boldsymbol{\psi}_0) \in \mathscr{V}$ such that

$$\mathscr{F}((\varphi_0, \boldsymbol{\psi}_0)) = \inf_{(\varphi,\boldsymbol{\psi})\in\mathscr{V}} \mathscr{F}((\varphi, \boldsymbol{\psi})), \tag{13}$$

where

$$\mathscr{F}((\varphi, \boldsymbol{\psi})) = \frac{1}{2}\int_\Omega \boldsymbol{\psi}\cdot\mathscr{A}[\boldsymbol{\psi}]\,\mathrm{d}a - \ell((\varphi, \boldsymbol{\psi})), \tag{14}$$

$$\ell((\varphi, \boldsymbol{\psi})) = \langle f, \varphi\rangle_{H^{-1},\, H_0^1}, \tag{15}$$

$$\mathscr{V} = \{(\varphi, \boldsymbol{\psi}) \in H_0^1(\Omega)\times (L^2(\Omega))^4 / \beta((\varphi, \boldsymbol{\psi}), \mathbf{q}) = 0, \quad \forall \mathbf{q} \in (H^1(\Omega))^4\}. \tag{16}$$

In (16), $\beta((\cdot,\cdot),\cdot)$ denotes the continuous bilinear form defined by

$$\forall(\varphi, \boldsymbol{\psi}) \in H^1(\Omega)\times(L^2(\Omega))^4, \quad \forall \mathbf{q} \in (H^1(\Omega))^4 : \beta((\varphi, \boldsymbol{\psi}), \mathbf{q}) = \int_\Omega \nabla\varphi\cdot\operatorname{div}\mathbf{q}\,\mathrm{d}a - \int_\Omega \boldsymbol{\psi}\cdot\mathbf{q}\,\mathrm{d}a. \tag{17}$$

Notice that the variational equation $\beta((\varphi, \boldsymbol{\psi}), \mathbf{q}) = 0$, $\forall \mathbf{q} \in (H^1(\Omega))^4$, implies that $\boldsymbol{\psi} = -\mathbf{H}\varphi$, with $\varphi \in H^2(\Omega)\cap H_0^1(\Omega)$, and $\partial\varphi/\partial n = 0$ over Γ (see Balasundaram and Bhattacharyya, 1986; Fraternali, 2001).

Now, consider a family of triangulations $\Pi_h = \{\Omega_1, \ldots, \Omega_M\}$ of Ω which are regular in the sense defined by Ciarlet (1978), $h = \sup_{m\in\{1,\ldots,M\}}\{\operatorname{diam}(\Omega_m)\}$ denoting the *mesh size*.

Associate a *dual mesh* $\widehat{\Pi}_h = \{\widehat{\Omega}_1, \ldots, \widehat{\Omega}_N\}$ to each triangulation Π_h, formed by N polygons, N being the number of nodes of Π_h. The vertices of the generic polygon $\widehat{\Omega}_n$ coincide with the middle points of the edges of Π_h that converge at the node $\mathbf{x}_n$, and with selected points in the interior of each triangles adjacent to $\mathbf{x}_n$ (Fig. 1).

Introduce also an extension Π_h' of Π_h outside Ω, obtained by adding a strip of external triangles, as shown in Fig. 1. In the following, Ω' denotes the open region covered by Π_h', and N' the number of nodes of Π_h'.

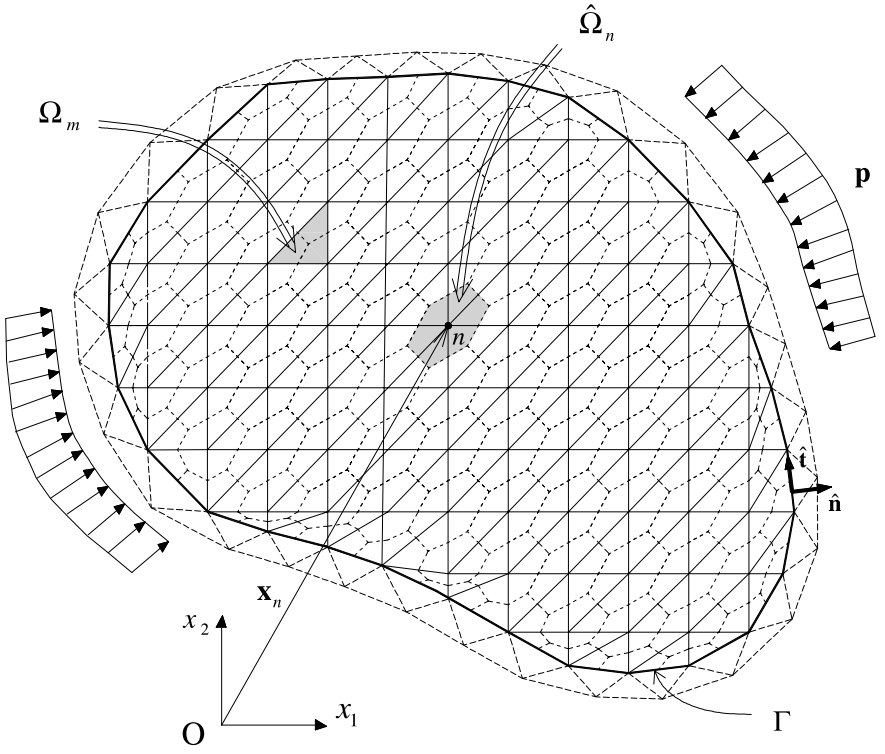

Fig. 1. Primal and dual meshes.

For a given mesh size h, we let S_h and T_h denote the space of piecewise linear scalar functions $\widehat{\varphi}$ defined over Π'_h (*polyhedral stress functions*), and the space of piecewise constant tensor-valued functions $\hat{\psi}$ defined over the dual mesh $\widehat{\Pi}_h$, respectively. In particular, we put $S_{0h} = \{\widehat{\varphi} \in S_h / \widehat{\varphi} = 0 \text{ on } \Omega' \setminus \Omega\}$.

The *natural basis* of S_h is the set of functions $\{\hat{g}_i\}_{i=1,\ldots,N'}$ which belong to such a finite-dimensional function space and are such that $\hat{g}_i(x_j) = \delta_{ij}$, $\forall j \in \{1, \ldots, N'\}$. Clearly, the support of $\hat{g}_i$ consists of the union G_i of the triangles which are adjacent to $\mathbf{x}_i$.

We call LSM the following approximation of problem (13).

Find $(\widehat{\varphi}_h, \widehat{\boldsymbol{\psi}}_h) \in \mathscr{W}_h$ such that

$$\mathscr{F}((\widehat{\varphi}_h, \widehat{\boldsymbol{\psi}}_h)) = \min_{(\widehat{\varphi}, \widehat{\boldsymbol{\psi}}) \mathscr{W}_h} \mathscr{F}((\widehat{\varphi}, \widehat{\boldsymbol{\psi}})), \tag{18}$$

with

$$\mathscr{W}_h = \{(\widehat{\varphi}, \widehat{\boldsymbol{\psi}}) \in S_{0h} \times T_h / \hat{\beta}((\widehat{\varphi}, \widehat{\boldsymbol{\psi}}), \hat{\mathbf{q}}) = 0, \quad \forall \hat{\mathbf{q}} \in T_h\}. \tag{19}$$

In the definition (19), $\hat{\beta}((\cdot,\cdot),\cdot)$ is the following approximation of the bilinear form (17)

$$\forall (\widehat{\varphi}, \widehat{\boldsymbol{\psi}}) \in S_h \times T_h, \ \forall \hat{\mathbf{q}} \in T_h : \hat{\beta}((\widehat{\varphi}, \widehat{\boldsymbol{\psi}}), \hat{\mathbf{q}}) = \int_\Omega \nabla \widehat{\varphi} \cdot \operatorname{div} \vartheta_h(\hat{\mathbf{q}}) \, \mathrm{d}a - \int_\Omega \widehat{\boldsymbol{\psi}} \cdot \hat{\mathbf{q}} \, \mathrm{d}a, \tag{20}$$

where $\vartheta_h(\hat{\mathbf{q}})$ is a piecewise linear function in $(S_h)^4$.

It is defined in the following way: *if* $\hat{\mathbf{q}} = \sum_{n=1}^{N} \hat{\mathbf{q}}(n)\chi_n$ *is in* T_h, $\hat{\mathbf{q}}(n)$ *being the value of* $\hat{\mathbf{q}}$ *over* $\widehat{\Omega}_n$ *and* χ_n *the characteristic function of* $\widehat{\Omega}_n$, *then* $\vartheta_h(\hat{\mathbf{q}})$ *is the function in* $(S_h)^4$ *such that*

$$\vartheta_h(\hat{\mathbf{q}})(\mathbf{x}_n) = \hat{\mathbf{q}}(n), \quad \forall n \in \{1,\dots,N\};\ \vartheta_h(\hat{\mathbf{q}}) = \mathbf{0} \text{ on } \partial\Omega'. \tag{21}$$

It is possible to show (Fraternali, 2001) that the couples $(\widehat{\varphi}, \widehat{\boldsymbol{\psi}})$ of the space $\mathscr{W}_h$ are such that

$$\widehat{\boldsymbol{\psi}} = -\mathbf{H}_h\widehat{\varphi} = -\sum_{n=1}^{N} \mathbf{H}_h\widehat{\varphi}(n)\chi_n, \tag{22}$$

where $\mathbf{H}_h\widehat{\varphi}$ is the *discrete hessian of* $\widehat{\varphi}$ defined through

$$(\mathbf{H}_h\widehat{\varphi}(n))_{\alpha\beta} = \frac{1}{|\widehat{\boldsymbol{\Omega}}_n|}\langle \widehat{\varphi}_{,\alpha\beta}, \hat{g}_n\rangle_{H^{-1},H_0^1}, \quad \forall n \in \{1,\dots,N\}. \tag{23}$$

The second derivatives $\widehat{\varphi}_{,\alpha\beta}$ are concentrated along the skeleton of the primal mesh. Indeed, say $\hat{\mathbf{h}}$ the unit normal to the generic inner edge Γ_n^s of Π_h', and put $\partial\widehat{\varphi}/\partial h = \nabla\widehat{\varphi}\cdot\hat{\mathbf{h}}$ $(\widehat{\varphi} \in S_{0h})$. A generalized second derivative $\partial^2\widehat{\varphi}/\partial h^2$ can be defined along Γ_n^s, as a linear Dirac delta. It's amplitude is equal to the jump $[[\partial\widehat{\varphi}/\partial h]]_n^s$ of $\partial\widehat{\varphi}/\partial h$ across Γ_n^s.

From (23), one can easily deduce that $\mathbf{H}_h\widehat{\varphi}(n)$ coincides with the mean value of the generalized Hessian $\mathbf{H}\widehat{\varphi}$ over the polygon $\widehat{\Omega}_n$, for each inner element of the dual mesh.

A similar result can be cited regarding dual elements associated with boundary nodes of Π_h, at the limit as the distance from Γ to the external nodes approaches zero (*penalization of the boundary condition* $\partial\widehat{\varphi}/\partial n = 0$).

Eq. (23) can also be written as

$$\mathbf{H}_h\widehat{\varphi} = -\frac{1}{|\widehat{\boldsymbol{\Omega}}_n|}\int_\Omega \nabla\widehat{\varphi}\otimes\nabla\hat{g}_n\,\mathrm{d}a, \tag{24}$$

and it results $|\widehat{\boldsymbol{\Omega}}_n| = \int_\Omega \hat{g}_n\,\mathrm{d}a,\ \forall n \in \{1,\dots,N\}$.

Introducing Eq. (22) into (14), we are led to the unconstrained problem

Find $\widehat{\varphi}_h \in S_{0h}$ such that

$$\mathscr{E}_h(\widehat{\varphi}_h) = \min_{\widehat{\varphi}\in S_{0h}} \mathscr{E}_h(\widehat{\varphi}), \tag{25}$$

with

$$\mathscr{E}_h(\widehat{\varphi}) = \frac{1}{2}\int_\Omega \mathbf{H}_h\widehat{\varphi}\cdot\mathscr{A}[\mathbf{H}_h\widehat{\varphi}]\,\mathrm{d}a - l_h(\widehat{\varphi}); \tag{26}$$

$$l_h(\widehat{\varphi}) = \langle f, \widehat{\varphi}\rangle_{H^{-1},H_0^1}. \tag{27}$$

We refer to $\mathscr{E}_h(\cdot)$ as a *relaxation* of $\mathscr{E}(\cdot)$ from $H_0^2(\Omega)$ to S_{0h}.

We have recently proved convergence of the sequence $\{(\widehat{\varphi}_h, \widehat{\psi}_h)\}$ to the weak solution $(\varphi_0, -\mathbf{H}\varphi_0)$ of the continuous problem (Fraternali, 2001).

We assumed that Π_h is regular in the sense of Ciarlet, $\widehat{\Pi}_h$ is formed by polygons with vertices at the centroids of primal elements (*barycentric dual mesh*), and Π_h has a *structured core*.

Concerning this last issue, we say that a node $\mathbf{x}_n$ satisfies the property $(\mathscr{P}_\Sigma)$ if, given an arbitrary tensor $\mathbf{H}$ (independent of position), it results

$$\sum_{\mathbf{x}_j\in\mathbf{X}_n}\int_{G_n} (\mathbf{H}(\mathbf{x}-\mathbf{x}_j)\cdot(\mathbf{x}-\mathbf{x}_j))\nabla\hat{g}_j\otimes\nabla\hat{g}_n = 0, \tag{28}$$

where $\mathbf{X}_n$ is set of nodes of the primal mesh that share a triangle with $\mathbf{x}_n$.

Such a geometrical property expands upon a similar one formulated by Glowinski (1973). It is not difficult to verify that it holds, for example, when G_n has one of the shapes shown in Fig. 2.

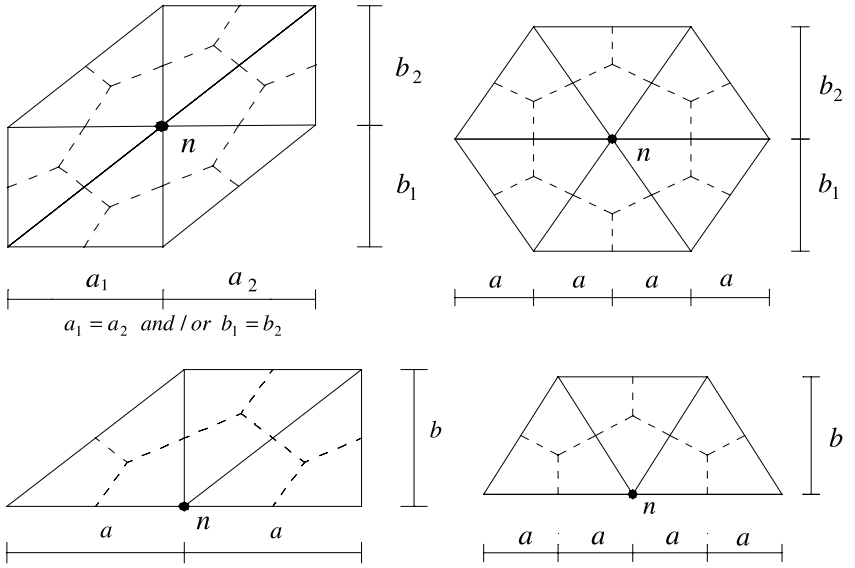

Fig. 2. Examples of nodes satisfying the ($\mathscr{P}_\Sigma$) property.

Now, let $|\Omega_{h_1}|$ denote the sum of the areas of the elements of $\widehat{\Pi}_h$ that contain nodes of Π_h satisfying the ($\mathscr{P}_\Sigma$) property, and set $|\Omega_{h_2}| = |\Omega| - |\Omega_{h_1}|$. Assume that

(i) the meshes $\{(\Pi_h, \widehat{\Pi}_h)\}$ are regular in the sense of Ciarlet;
(ii) the dual meshes $\widehat{\Pi}_h$ are barycentric;
(iii) $|\Omega_{h_2}| \to 0$ as $h \to 0$;
(iv) φ_0 belongs to the Sobolev space $H^4(\Omega) \cap W^{3,\infty}(\Omega) \cap H_0^2(\Omega)$.

Under the above assumptions, we have deduced the following error estimate

$$e_h = |\varphi_0 - \widehat{\varphi}_h|_1 + \|\mathbf{H}\varphi_0 - \mathbf{H}_h\widehat{\varphi}_h\|_0 \leqslant c_1 h\|\varphi_0\|_{3,\infty} + c_2 h^{1/2}\|\varphi_0\|_4, \tag{29}$$

where $\|\cdot\|_k$ denotes the usual norm in $H^k(\Omega)$; $|\cdot|_1$ the seminorm in $H^1(\Omega)$; $\|\cdot\|_{3,\infty}$ the norm in $W^{3,\infty}(\Omega)$; and c_1, c_2 are constants independent of φ_0 and h.

In particular, when (iii) and (iv) are replaced by $|\Omega_{h_2}| \leqslant \bar{c}h^2$ (with $\bar{c}$ independent of h) and $\varphi_0 \in W^{4,\infty}(\Omega) \cap H_0^2(\Omega)$, respectively, we have proved that there exists a constant c independent of φ_0 and h such that

$$e_h \leqslant ch\|\varphi_0\|_{4,\infty}. \tag{30}$$

The estimate (29) is useful when the core of Π_h is formed by nodes satisfying the ($\mathscr{P}_\Sigma$) property, and the nodes that do verify such a property are confined to a strip adjacent to the boundary of Ω (see, e.g., Fig. 1). Indeed, in this case, $|\Omega_{h_2}|$ is of $O(h)$.

The estimate (30) is instead useful when Ω coincides with a rectangular region and the meshes $\{(\Pi_h, \widehat{\Pi}_h)\}$ are generated by structured grids of nodes. In such a situation, all the nodes of Π_h satisfy the ($\mathscr{P}_\Sigma$) property, with exception to the four corner nodes, and thus $|\Omega_{h_2}|$ is of $O(h^2)$.

Notice that the above error estimates do not imply any particular hypothesis about the *orientation* of the primal mesh.

2.4. The general case with mixed boundary conditions

Let us now consider the case in which the boundary Γ can be divided into a free part, Γ_p, and a constrained part, $\Gamma_u = \Gamma \setminus \Gamma_p$, where given displacements $\bar{\mathbf{u}} \in C^0(\Gamma_u)$ are prescribed.

From now on $\mathbf{T}^*$ is a stress field which satisfies the indefinite equilibrium equation $\mathrm{div}\,\mathbf{T}^* + \mathbf{b} = \mathbf{0}$ and is free to assume arbitrary values on Γ.

Assume that the load $(\mathbf{b}, \mathbf{p})$ is regular enough to ensure that the following functions on Γ_p

$$\mu(\sigma) = \hat{\mathbf{e}}_3 \cdot \int_0^\sigma (\mathbf{x}(s) - \mathbf{x}(\sigma)) \times (\mathbf{p} - \mathbf{T}^*\hat{\mathbf{n}})\,\mathrm{d}s, \tag{31}$$

$$\tau(\sigma) = \hat{\mathbf{t}}(\sigma) \cdot \int_0^\sigma (\mathbf{p} - \mathbf{T}^*\hat{\mathbf{n}})\,\mathrm{d}s, \tag{32}$$

are such that $\mu \in C^0(\Gamma_p)$, and τ is either in $C^0(\Gamma_p)$ or is piecewise continuous over Γ_p. In (30)–(32), σ is the arc length of Γ measured by some origin O', $\hat{\mathbf{t}}$ is the unit tangent to Γ, and $\hat{\mathbf{e}}_3$ is the out-plane unit vector such that $\{\hat{\mathbf{e}}_1, \hat{\mathbf{e}}_2, \hat{\mathbf{e}}_3\}$ forms a right-handed basis.

The boundary value problem corresponding to the present situation can be expressed in the following variational form

Find $\varphi_0 \in H_p^2(\Omega)$ such that

$$\mathscr{E}(\varphi_0) = \inf_{\varphi \in H_p^2(\Omega)} \mathscr{E}(\varphi), \tag{33}$$

where

$$H_p^2(\Omega) = \left\{ \varphi \in H^2(\Omega) / \varphi = \mu,\ \frac{\partial \varphi}{\partial n} = -\tau \text{ on } \Gamma_p \right\}, \tag{34}$$

$$\mathscr{E}(\varphi) = \frac{1}{2} \int_\Omega \mathbf{H}\varphi \cdot \mathscr{A}[\mathbf{H}\varphi]\,\mathrm{d}\boldsymbol{a} - \boldsymbol{l}(\varphi), \tag{35}$$

with

$$l(\varphi) = -\int_\Omega (\mathbf{WH}\varphi\mathbf{W}^{\mathrm{T}}) \cdot (\overline{\mathbf{E}} + \mathbf{A}[\mathbf{T}^*])\,\mathrm{d}a + \langle (\mathbf{WH}\varphi\mathbf{W}^{\mathrm{T}})\hat{\mathbf{n}}, \bar{\mathbf{u}} \rangle_\Gamma, \tag{36}$$

$\langle \cdot, \cdot \rangle_\Gamma$ denoting the duality pairing between $(H^{-1/2}(\Gamma))^2$ and $(H^{1/2}(\Gamma))^2$. Notice that, for a $\varphi \in H^2(\Omega)$, the tensor field $\mathbf{WH}\varphi\mathbf{W}^{\mathrm{T}}$ is in the space $H(\mathrm{div}, \Omega) = \{\mathbf{T} \in (L^2(\Omega))^4 / \mathrm{div}\mathbf{T} \in (L^2(\Omega))^2\}$, as it is easily observed. Thus, the trace of such a field on Γ exists and is an element of $(H^{-1/2}(\Gamma))^2$ (cf. Lions and Magenes, 1968; Ciarlet, 1978).

In order to extend the LSM of Section 2.3, consider again a primal triangular mesh Π_h over Ω, a dual polygonal mesh $\widehat{\Pi}_h$, and an extension Π'_h form Π_h obtained by introducing external triangles in correspondence with the portion Γ_p of the boundary (Fig. 3). Let I, P and U indicate the sets of the indices of the nodes of Π_h which lie in the interior of Ω, along Γ_p, and along Γ_u, respectively, and let Ω' be the open region covered by Π'_h.

Moreover, along Γ_p, consider a piecewise linear interpolant $\hat{\mu}$ of the function (31), and a piecewise constant interpolant $\hat{\tau}$ of the function (32). The latter being such that its value over the generic edge of Γ_p is equal to the value of τ in correspondence with the middle point.

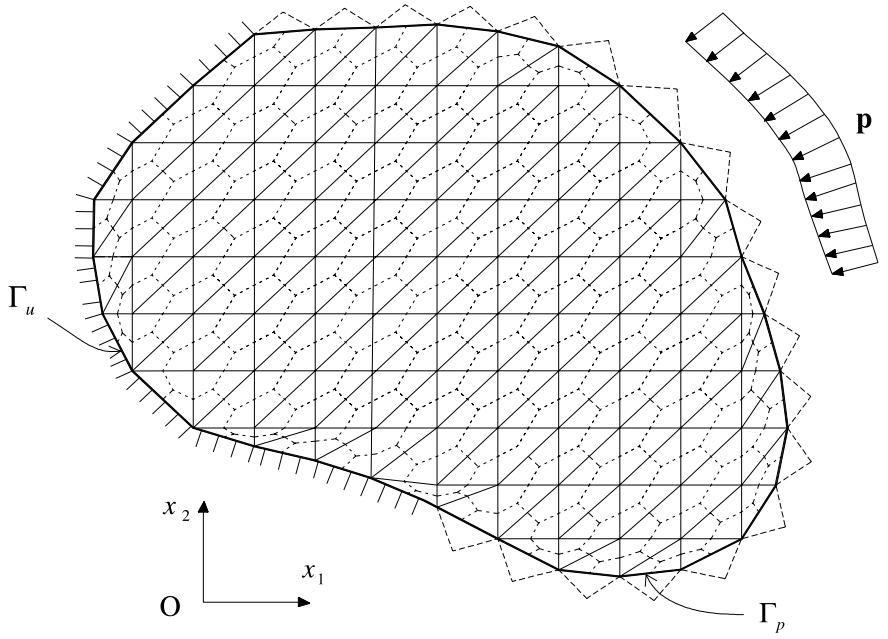

Fig. 3. Primal and dual meshes for a problem with mixed boundary conditions.

Upon introducing the following space of piecewise linear functions over Π'_h

$$S_{ph} = \{\varphi \in \mathrm{C}^0(\Omega')/\text{the restriction } \widehat{\varphi}|_{\Omega_m} \text{ is linear for each triangle } \Omega_m \in \Pi'_h, \\ \widehat{\varphi} = \hat{\mu} \text{ on } \Gamma_p, \nabla\widehat{\varphi}\cdot\hat{\mathbf{n}} = -\hat{\tau} \text{ over } \Pi'_h/\Pi_h\}, \tag{37}$$

a LSM for problem (33) can be formulated as follows

Find $\widehat{\varphi}_h \in S_{ph}$ such that

$$\mathscr{E}_h(\widehat{\varphi}_h) = \inf_{\widehat{\varphi}\in S_{ph}} \mathscr{E}_h(\widehat{\varphi}), \tag{38}$$

where

$$\mathscr{E}_h(\widehat{\varphi}) = \frac{1}{2}\int_\Omega \mathbf{H}_h\widehat{\varphi}\cdot\mathscr{A}[\mathbf{H}_h\widehat{\varphi}]\,\mathrm{d}a - l_h(\widehat{\varphi}), \tag{39}$$

with

$$\mathbf{H}_h\widehat{\varphi} = \sum_{n=1}^{N}\frac{\chi_n}{|\widehat{\Omega}_n|}\sum_{s=1}^{\mathscr{S}_n}\frac{\ell_n^s}{2}\left[\left[\frac{\partial\widehat{\varphi}}{\partial h}\right]\right]_n^s \hat{\mathbf{h}}_n^s\otimes\hat{\mathbf{h}}_n^s; \tag{40}$$

$$l_h(\widehat{\varphi}) = -\sum_{\Gamma_n^s\in\Sigma_h}\left[\left[\frac{\partial\widehat{\varphi}}{\partial h}\right]\right]_n^s\bar{\Delta}_n^s - \sum_{n\in U}\bar{\mathbf{u}}(\mathbf{x}_n)\cdot\left(\sum_{s=1}^{S_n}\left[\left[\frac{\partial\widehat{\varphi}}{\partial h}\right]\right]_n^s\hat{k}_n^s\right). \tag{41}$$

In (40) and (41), $\Gamma_n^1,\ldots,\Gamma_n^{\mathscr{S}_n}$ denote the edges of the primal mesh which are incident to $\mathbf{x}_n$ and lie in the interior of $\overline{\Omega'}$; ℓ_n^s denotes the length of Γ_n^s; $\hat{\mathbf{k}}_n^s$ and $\hat{\mathbf{h}}_n^s$ respectively indicate the unit tangent and the unit normal to Γ_n^s (Fig. 4). Moreover, $[[\partial\widehat{\varphi}/\partial h]]_n^s$ denotes the jump of $\nabla\widehat{\varphi}\cdot\hat{\mathbf{h}}_n^s$ through Γ_n^s; Σ_h the set of the edges Γ_n^s (i.e., the *skeleton* of the primal mesh); and $\bar{\Delta}_n^s$ the quantity defined by

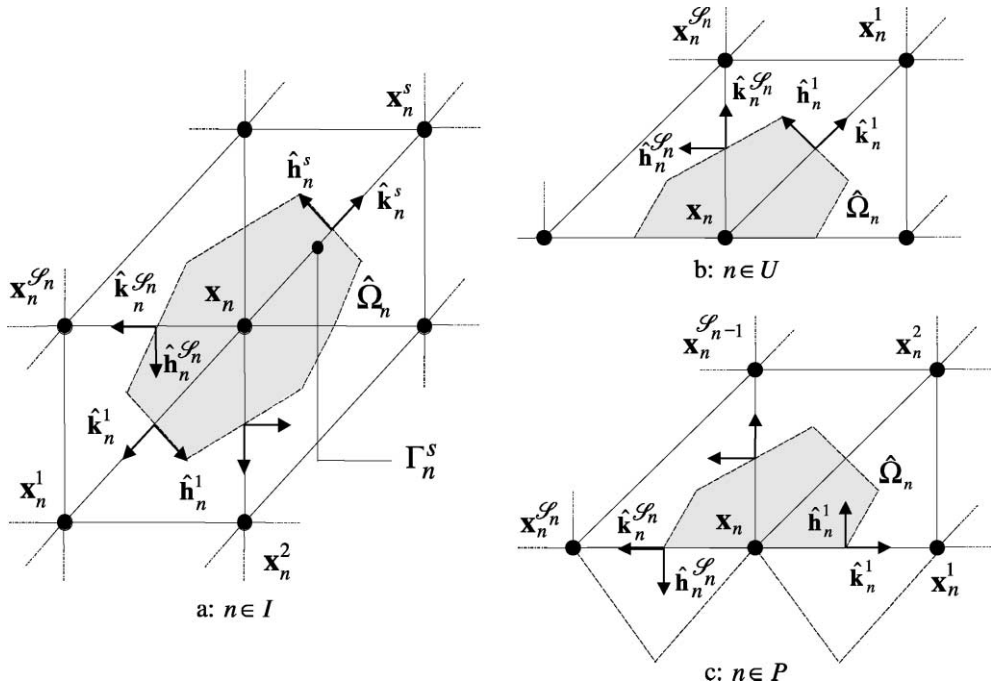

Fig. 4. Details of inner and boundary nodes of the primal mesh.

$$\bar{\Lambda}_n^s = \hat{\mathbf{k}}_n^s \otimes \hat{\mathbf{k}}_n^s \cdot \int_{\Gamma_n^s} (\overline{\mathbf{E}} + \mathbf{A}[\mathbf{T}^*])\, \mathrm{d}\sigma. \tag{42}$$

Thus, one can write $\mathscr{E}_h(\cdot)$ as follows

$$\forall \widehat{\varphi} \in S_{ph} : \mathscr{E}_h(\widehat{\varphi}) = \frac{1}{2} \sum_{n=1}^{N} \sum_{s,t=1}^{S_n} \hat{A}_n^{st} \left[\left[\frac{\partial \widehat{\varphi}}{\partial h}\right]\right]_n^s \left[\left[\frac{\partial \widehat{\varphi}}{\partial h}\right]\right]_n^t + \sum_{\Gamma_n^s \in \Sigma_h} \left[\left[\frac{\partial \widehat{\varphi}}{\partial h}\right]\right]_n^s \bar{\Lambda}_n^s + \sum_{n \in U} \bar{\mathbf{u}}(\mathbf{x}_n) \cdot \left(\sum_{s=1}^{S_n} \left[\left[\frac{\partial \widehat{\varphi}}{\partial h}\right]\right]_n^s \hat{\mathbf{k}}_n^s \right), \tag{43}$$

where

$$\hat{A}_n^{st} = \frac{\ell_n^s \ell_n^t \mathscr{A}[\hat{\mathbf{h}}_n^s \otimes \hat{\mathbf{h}}_n^s] \cdot \hat{\mathbf{h}}_n^t \otimes \hat{\mathbf{h}}_n^t}{4|\widehat{\Omega}_n|} = \frac{\ell_n^s \ell_n^t \mathbf{A}[\hat{\mathbf{k}}_n^s \otimes \hat{\mathbf{k}}_n^s] \cdot \hat{\mathbf{k}}_n^t \otimes \hat{\mathbf{k}}_n^t}{4|\widehat{\Omega}_n|}. \tag{44}$$

3. Numerical implementation

Given a polyhedral stress function $\widehat{\varphi} \in S_{ph}$, each one of the slope jumps $[[\partial \widehat{\varphi}/\partial h]]_n^s$ can be expressed as a linear combination of the differences between the values of $\widehat{\varphi}$ at the nodes connected to $\mathbf{x}_n$, and the value of $\widehat{\varphi}$ at $\mathbf{x}_n$. That is,

$$\left[\left[\frac{\partial \widehat{\varphi}}{\partial h}\right]\right]_n^s = \sum_{t=1}^{\mathscr{S}'_n} C_n^{st} \left(\widehat{\varphi}_n^t - \widehat{\varphi}_n\right), \quad s = 1, \ldots, \mathscr{S}_n, \tag{45}$$

C_n^{st} being suitable $\mathscr{S}'_n \times \mathscr{S}_n$ coefficients ($\mathscr{S}'_n = \mathscr{S}_n$, for $n \in I$).

The use of (45) into (43) leads one to get

$$\mathscr{E}_h(\widehat{\varphi}) = \frac{1}{2}\mathbf{F}\hat{\boldsymbol{\varphi}}\cdot\hat{\boldsymbol{\varphi}} - \mathbf{g}\cdot\hat{\boldsymbol{\varphi}}, \tag{46}$$

where $\hat{\boldsymbol{\varphi}} = \{\widehat{\varphi}_n\}_{n=1,\ldots,N'}$ is the vector collecting the nodal values of $\widehat{\varphi}$, $\mathbf{F}$ is a $N'\times N'$ matrix (*flexibility matrix*), and $\mathbf{g}$ is a vector of $\Re^{N'}$.

Thus, the minimizer $\widehat{\varphi}_h$ of $\mathscr{E}_h(\widehat{\varphi})$ over S_{ph} corresponds with the solution $\hat{\boldsymbol{\varphi}}_h$ of the linear system

$$\mathbf{F}\hat{\boldsymbol{\varphi}} = \mathbf{g}. \tag{47}$$

Eq. (47) defines the SFF of the LSM.

Observe that the calculation of $\mathbf{F}$ and $\mathbf{g}$ just requires sum and assembling operations, and not numerical integrations. In particular, $\mathbf{F}$ has a highly sparse structure. This is also because each primal triangle requires only three degrees of freedom (one per node), that is one half of the DOF required by a constant-strain triangle of a standard (displacement-based) finite element model, and one sixth of the DOF required by a T18 composite triangle (C^1 approximation of the stress function, cf. Oden and Carey, 1983a).

4. Truss analogy

The stress approximation induced by the SFF is of the form

$$\mathbf{T} = \mathbf{T}^* + \mathbf{T}_h\widehat{\varphi}, \tag{48}$$

where $\mathbf{T}_h\widehat{\varphi} = \mathbf{W}^{\mathrm{T}}\mathbf{H}_h\widehat{\varphi}\mathbf{W}$ is a piecewise constant stress field associated to the polyhedral stress function $\widehat{\varphi}\in S_{ph}$. According to (40), the value of $\mathbf{T}_h\widehat{\varphi}$ over the generic dual element $\widehat{\Omega}_n$ is given by

$$\mathbf{T}_h\widehat{\varphi}(n) = \frac{1}{|\widehat{\Omega}_n|}\sum_{s=1}^{\mathscr{S}_n}\frac{\ell_n^s}{2}\left[\left[\frac{\partial\widehat{\varphi}}{\partial h}\right]\right]_n^s \hat{\mathbf{k}}_n^s\otimes\hat{\mathbf{k}}_n^s. \tag{49}$$

The quantity $[[\partial\widehat{\varphi}/\partial h]]_n^s$ dimensionally represents a force per unit thickness of the body. It can be identified with the resultant of the normal stress $\sigma_n^s = (\mathbf{T}-\mathbf{T}^*)\hat{\mathbf{k}}_n^s\cdot\hat{\mathbf{k}}_n^s$ over the generic cross section of the plane region $\widehat{\Omega}_n^s$ shown in Fig. 5.

Now, introduce an ideal *truss structure* $\mathscr{B}_h$ having the same topology of the skeleton of the primal mesh (the set Σ_h of the interfaces Γ_n^s lying in the interior of $\overline{\Omega'}$), and denote P_n^s the axial force in the bar aligned with Γ_n^s.

Upon setting $P_n^s(\widehat{\varphi}) = [[\partial\widehat{\varphi}/\partial h]]_n^s$ (Fig. 5), it is not difficult to verify that an arbitrary $\widehat{\varphi}\in S_{ph}$ generates a set of balanced axial forces in $\mathscr{B}_h$, i.e., a set of forces such that

$$\begin{cases}\sum_{s=1}^{\mathscr{S}_n} P_n^s(\widehat{\varphi})\hat{\mathbf{k}}_n^s = \mathbf{0}, & \forall n\in I,\\ \sum_{s=1}^{\mathscr{S}_n} P_n^s(\widehat{\varphi})\hat{\mathbf{k}}_n^s + \mathbf{Q}_n = \mathbf{0}, & \forall n\in P,\end{cases} \tag{50}$$

where

$$\mathbf{Q}_n = \left[\left[\frac{\partial\widehat{\varphi}}{\partial\sigma}\hat{\mathbf{n}} - \frac{\partial\widehat{\varphi}}{\partial n}\hat{\mathbf{t}}\right]\right]_n, \tag{51}$$

$[[\cdot]]_n$ denoting the jump of $(\cdot)$ across the external triangles incident to n (Fig. 4(c)). Clearly, the boundary forces $\{\mathbf{Q}_n\}_{n\in P}$ correspond to the surface tractions $\mathbf{p}-\mathbf{T}^*\hat{\mathbf{n}}$ over Γ_p (see Eqs. (31), (32) and (37)). Eq. (49) establishes a correspondence between the set of axial forces generated in $\mathscr{B}_h$ by $\widehat{\varphi}\in S_{ph}$, and the piecewise continuous approximation of the stress field $\mathbf{T}_h\widehat{\varphi} = \mathbf{T}-\mathbf{T}^*$. It relates $\mathbf{T}_h\widehat{\varphi}(n)$ with a weighted (tensorial) sum of the axial forces intercepted by $\widehat{\Omega}_n$.

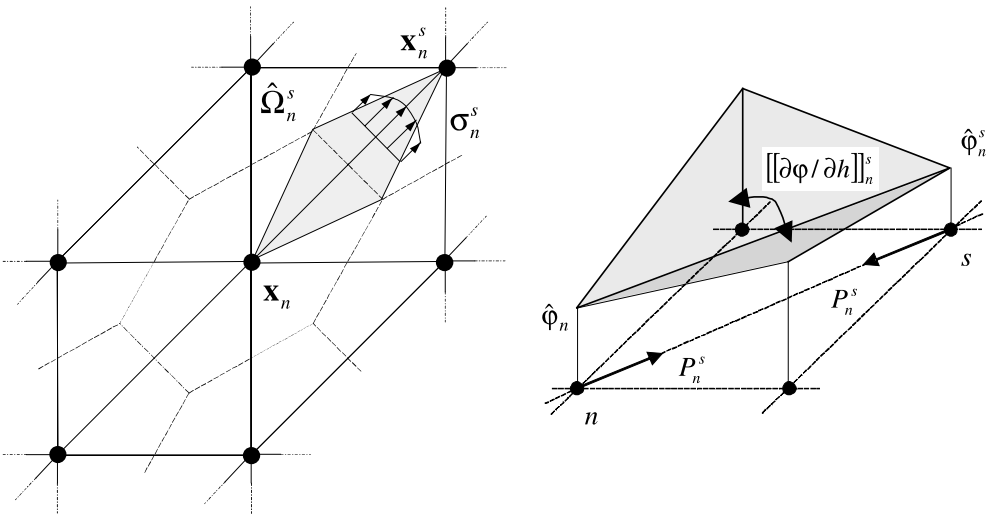

Fig. 5. Axial force P_n^s associated with a polyhedral stress function $\widehat{\varphi}$.

The truss $\mathscr{B}_h$ is supported in correspondence with the nodes lying on Γ_u. For a given $\widehat{\varphi} \in S_{ph}$, the *support reactions* balanced with $P_n^s(\widehat{\varphi})$ are given by (Fig. 4(b))

$$\mathbf{R}_n(\widehat{\varphi}) = -\sum_{s=1}^{S_n} P_n^s(\widehat{\varphi})\hat{\mathbf{k}}_n^s, \quad \forall n \in U. \tag{52}$$

Now, let N_Γ denote the number of interfaces Γ_n^s, N_U the dimension of the set U, and $\mathbf{P}(\hat{\boldsymbol{\varphi}}) \in \mathfrak{R}^{N_\Gamma}$ the vector collecting scalar quantities $P_n^s(\widehat{\varphi})$. According to Eq. (43), we can write

$$\mathscr{E}_h(\hat{\boldsymbol{\varphi}}) = \frac{1}{2}\mathbf{P}(\hat{\boldsymbol{\varphi}}) \cdot \hat{\mathbf{A}}\mathbf{P}(\hat{\boldsymbol{\varphi}}) + \mathbf{P}(\hat{\boldsymbol{\varphi}}) \cdot \bar{\Delta} - \mathbf{R}(\hat{\boldsymbol{\varphi}}) \cdot \overline{\mathbf{U}}, \tag{53}$$

where

$\hat{\mathbf{A}}$ is a $N_\Gamma \times N_\Gamma$ *compliance matrix*, obtained by assembling the quantities $\hat{A}_n^{st}$ defined as in (44);
$\bar{\Delta} \in \mathfrak{R}^{N_\Gamma}$ is the *vector of the initial bar extensions*, collecting the quantities $\bar{\Delta}_n^s$ defined as in (42);
$\overline{\mathbf{U}} \in \mathfrak{R}^{2N_u}$ is the *vector of the prescribed nodal displacements* $\bar{\mathbf{u}}(\mathbf{x}_n)$ $(n \in U)$;
$\mathbf{R}(\hat{\boldsymbol{\varphi}}) \in \mathfrak{R}^{2N_u}$ is the *vector of the support reactions*, collecting the quantities $\mathbf{R}_n(\widehat{\varphi})$.

Thus, the relaxed energy $\mathscr{E}_h(\hat{\boldsymbol{\varphi}})$ can be interpreted as *the complementary energy* induced by the axial forces $P_n^s(\widehat{\varphi})$ in the truss $\mathscr{B}_h$.

It differs from the complementary energy of a real truss structure due to the form of the *stress energy* $1/2\mathbf{P} \cdot \hat{\mathbf{A}}\mathbf{P}$, which is defined per dual elements and not per bar elements. This energy couples the elastic effects of the axial forces converging to the same node, in such a way that $\mathscr{B}_h$ reproduces the behavior of the continuous body as $h \to 0$ (see the error estimates of Section 2.3 and the numerical results of Section 6). It is worth noting that, in general, an analogous result cannot be obtained by replacing the body with a conventional truss structure.

5. Nodal displacement formulation

We want to show in this section that: (i) the stationary conditions of the relaxed energy (53) yield axial forces in the truss $\mathscr{B}_h$ which are compatible with a vector of nodal displacements $\mathbf{U} \in \mathfrak{R}^{2(N-N_u)}$; (ii) such a vector can be assumed as the independent variable of the LSM.

We begin observing that Eq. (50) can be written into the following matrix form

$$\mathbf{SP} + \mathbf{Q} = \mathbf{0}, \tag{54}$$

$\mathbf{S}$ being the *static matrix* of the truss $\mathscr{B}_h$, with $2(N + N_u)$ rows and N_Γ columns. In (54), $\mathbf{Q}$ is the vector of $\mathfrak{R}^{2(N-N_u)}$ with a couple of zero entries for each $n \in I$, and two entries equal to the Cartesian components of $\mathbf{Q}_n$ for each $n \in P$.

Similarly, Eq. (52) can be written as

$$\mathbf{R} = -\overline{\mathbf{S}}\mathbf{P}, \tag{55}$$

$\overline{\mathbf{S}}$ being a second static matrix, with $2N_u$ rows and N_Γ columns.

If the axial forces P_n^s are taken as primal variables of the LSM, the following constrained problem has to be considered

$$\begin{cases} \underset{\mathbf{P}\in\mathfrak{R}^{N_\Gamma}}{\text{minimize}} & \tilde{\mathscr{E}}_h(\mathbf{P}) = \frac{1}{2}\mathbf{P}\cdot\hat{\mathbf{A}}\mathbf{P} + \mathbf{P}\cdot\bar{\Delta} + \overline{\mathbf{S}}\mathbf{P}\cdot\overline{\mathbf{U}}, \\ \text{subject to} & \mathbf{SP} + \mathbf{Q} = \mathbf{0}. \end{cases} \tag{56}$$

This can be addressed by searching for the stationary point $(\mathbf{P}_h, \lambda_h)$ of the *Lagrangian function*

$$\mathscr{L}_h(\mathbf{P}, \lambda) = \tilde{\mathscr{E}}_h(\mathbf{P}) - \lambda\cdot(\mathbf{SP} + \mathbf{Q}), \tag{57}$$

where $\lambda \in \mathfrak{R}^{2(N+N_u)}$ is the vector of the Lagrange multipliers. The optimality conditions of $\mathscr{L}_h(\mathbf{P}, \lambda)$ are

$$\begin{cases} \hat{\mathbf{A}}\mathbf{P} + \bar{\Delta} = \mathbf{S}^{\mathrm{T}}\lambda - \overline{\mathbf{S}}^{\mathrm{T}}\overline{\mathbf{U}}, \\ \mathbf{SP} + \mathbf{Q} = \mathbf{0}. \end{cases} \tag{58}$$

Recalling standard results about the kinematics of truss structures, it is easy to recognize that the matrices $\mathbf{C} = \mathbf{S}^{\mathrm{T}}$ and $\overline{\mathbf{C}} = \overline{\mathbf{S}}^{\mathrm{T}}$ rule the *geometrical problem* of $\mathscr{B}_h$, that is, the search for the *free nodal displacements* $\mathbf{U} \in \mathfrak{R}^{2(N-N_u)}$ that solve the linear system

$$\mathbf{CU} + \overline{\mathbf{C}}\,\overline{\mathbf{U}} = -\hat{\Delta}, \tag{59}$$

for given $\overline{\mathbf{U}} \in \mathfrak{R}^{2N_u}$ and $\Delta \in \mathfrak{R}^{N_\Gamma}$.

Comparing $(58)_1$ with (59) we can deduce that the solution $\mathbf{P}_h$ is kinematically compatible with the following nodal displacements and bar elongations

$$\begin{cases} \mathbf{U}_h = -\lambda_h, \\ \Delta_h = \hat{\mathbf{A}}\mathbf{P}_h + \bar{\Delta}. \end{cases} \tag{60}$$

Therefore, we can rearrange our approximation scheme, assuming $\mathbf{U}$ as the independent variable and searching for the solution of equilibrium equations (54) in the following set of axial forces

$$\mathbf{P} = \hat{\mathbf{A}}^{-1}(\mathbf{CU} + \overline{\mathbf{C}}\,\overline{\mathbf{U}} - \bar{\Delta}), \tag{61}$$

The substitution of (61) into (54) yields the linear system

$$\mathbf{KU} + \mathbf{q} = \mathbf{0}, \tag{62}$$

where

$$\mathbf{K} = \mathbf{C}^{\mathrm{T}}\hat{\mathbf{A}}^{-1}\mathbf{C} \tag{63}$$

is the *stiffness matrix* of $\mathscr{B}_h$, and

$$\mathbf{q} = \mathbf{Q} + \mathbf{C}^{\mathrm{T}}\hat{\mathbf{A}}^{-1}\mathbf{C}\overline{\mathbf{U}} - \mathbf{C}^{\mathrm{T}}\hat{\mathbf{A}}^{-1}\bar{\Delta} \tag{64}$$

is the *nodal force vector*.

The matrix equation (62) defines the *nodal displacement formulation* (NDF) of the LSM. It can be usefully employed to analyze multiple-connected bodies (see the Example 6 of Section 6) and to integrate the LSM with displacement-based procedures, such as standard finite element approximations. In particular, it allows one to treat body forces in a simple form since such forces can be directly assembled into $\mathbf{q}$. Notice that the NDF represents a displacement approach to a stress-based approximation of the 2D problem, since it produces statically admissible solutions for each size of the discrete problem, as well as the SFF.

Differing from the flexibility matrix $\mathbf{F}$, the stiffness matrix $\mathbf{K}$ is generally dense.

6. Numerical results

Using the LSM we analyzed some significant problems of 2D elasticity, employing meshes with different sizes and orientations.

A first group of problems (Examples 1–5) were analyzed by means of the SFF, through the following steps:

(a) computation of the nodal values of the stress function by the sparse linear system $\mathbf{F}\hat{\boldsymbol{\varphi}} = \mathbf{g}$;
(b) computation of the approximating force network by the equations $P_n^s = [[\partial\widehat{\varphi}/\partial h]]_n^s$;
(c) approximation of the stress field through the piecewise constant field $\mathbf{T}_h$ such that

$$\mathbf{T}_h(n) = \frac{1}{|\widehat{\Omega}_n|}\sum_{s=S_1}^{S_2}\frac{\ell_n^s}{2}P_n^s\hat{\mathbf{k}}_n^s \otimes \hat{\mathbf{k}}_n^s;$$

(d) computation of the nodal displacements of the truss $\mathscr{B}_h$ by $\mathbf{CU} = \hat{\mathbf{A}}\mathbf{P} + \bar{\Delta} - \overline{\mathbf{C}}\,\overline{\mathbf{U}}$;
(e) smoothing of the discrete approximations through piecewise cubic interpolation and construction of regularized functions $\tilde{\varphi}_h$, $\tilde{\mathbf{T}}_h$ and $\tilde{\mathbf{u}}_h$.

In particular, the linear system of point (d) was worked out by calculating the Moore–Penrose generalized inverse of the rectangular matrix $\mathbf{C}$ (see, e.g., Campbell and Meyer, 1991). Smoothing of output data and most of the graphic manipulations of the results were performed by *Mathematica*® (Wolfram, 1991). Specific graphic software for managing the LSM (Rocchetta, 2000) was also used.

The final example (Example 6) concerns the NDF of the LSM. The following procedure was employed:

(a) computation of the compliance matrix $\hat{\mathbf{A}}$ of the truss $\mathscr{B}_h$;
(b) inversion of $\hat{\mathbf{A}}$;
(c) computation of the stiffness matrix $\mathbf{K} = \mathbf{C}^{\mathrm{T}}\hat{\mathbf{A}}^{-1}\mathbf{C}$;
(d) solution of the linear system $\mathbf{KU} + \mathbf{q} = \mathbf{0}$;
(e) computation of the approximating force network by $\mathbf{P} = \hat{\mathbf{A}}^{-1}(\mathbf{CU} + \overline{\mathbf{C}}\,\overline{\mathbf{U}} - \bar{\Delta})$;
(f) construction of the piecewise constant stress approximation $\mathbf{T}_h$;
(g) smoothing of the discrete approximations and construction of regularized functions $\tilde{\mathbf{T}}_h$ and $\tilde{\mathbf{u}}_h$.

Use was made of primal and dual meshes satisfying the regularity properties discussed in Section 2.3.

6.1. Examples 1, 2, 3—Convergence study

Fig. 6(a)–(c) show three sample problems of 2D elasticity, exhibiting "exact" (or analytic) C^{∞} solutions. The first deals with the traction problem of a wall-beam composed of an isotropic material. The second and third refer instead to a traction problem and a displacement problem (simple shear) of a body composed of an orthotropic material, whose symmetry axes (x_1', x_2') are rotated by 30° with respect to the Cartesian axes (x_1, x_2).

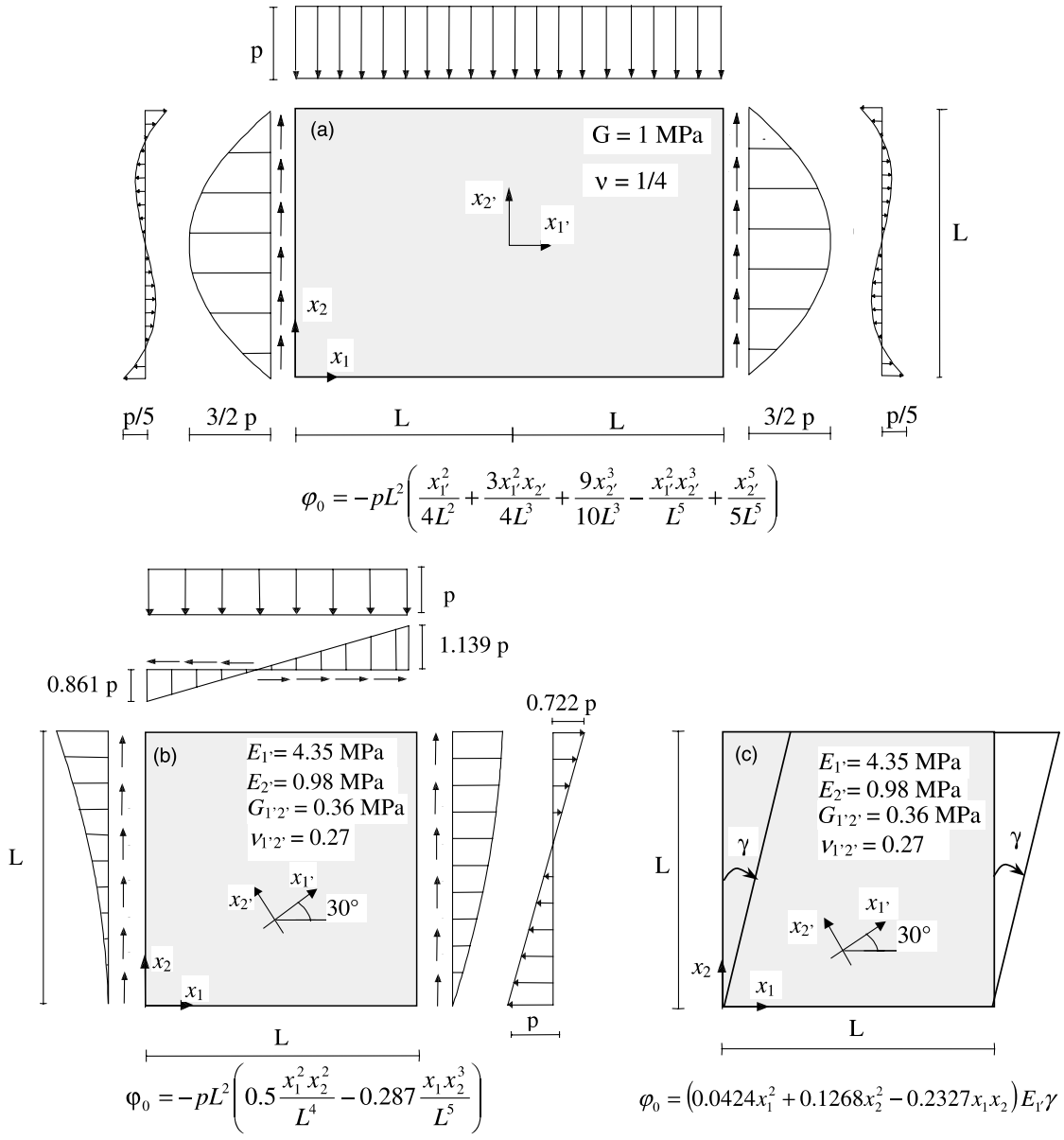

Fig. 6. (a)–(c) Examples 1–3 analyzed by the LSM and corresponding exact solutions for the Airy function.

For each of these problems, we performed a numerical convergence study of the LSM for decreasing values of the mesh size h. Triangulations generated by equally spaced grids of nodes were adopted as primal meshes. We recall that the use of such meshes ensures a $O(h)$-convergence of the LSM in the case of traction problems (cf. Section 2.3).

Fig. 7(a)–(c) show the polyhedral stress functions $\widehat{\varphi}_h$ and the deformed shapes exhibited by the LSM when a 10×10 mesh is employed. Figs. 8–10 instead show a comparison between the contours of

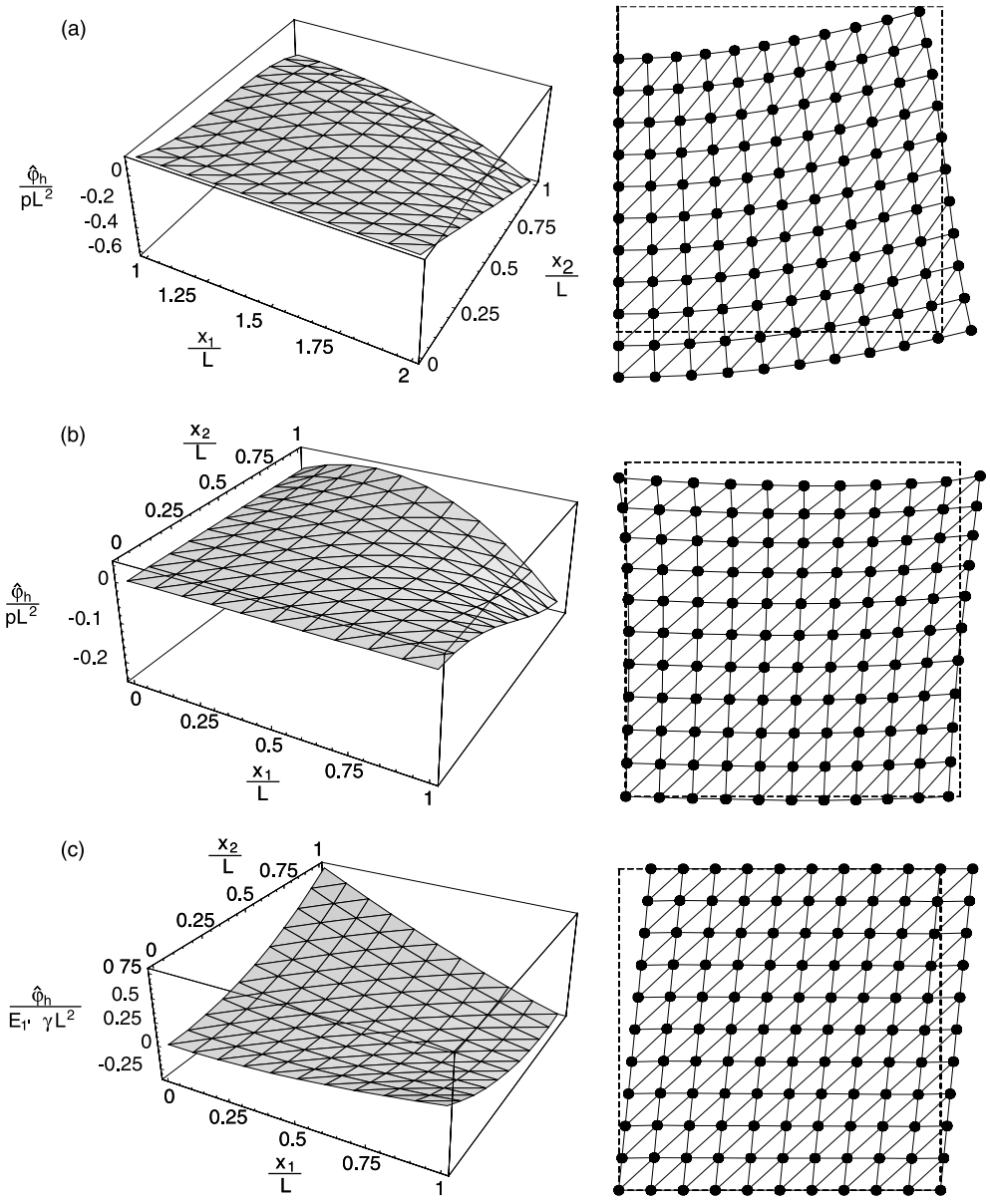

Fig. 7. (a)–(c) Polyhedral stress functions (*left*) and deformed shapes (*right*) given by the LSM (SFF) for the Examples 1 (*top*), 2 (*middle*), and 3 (*bottom*). (– – – –) $h = 0.25L$ (25 DOF); (– – – –) $h = 0.10L$ (121 DOF); (- - - - - - -) $h = 0.05L$ (441 DOF); (—) exact solution.

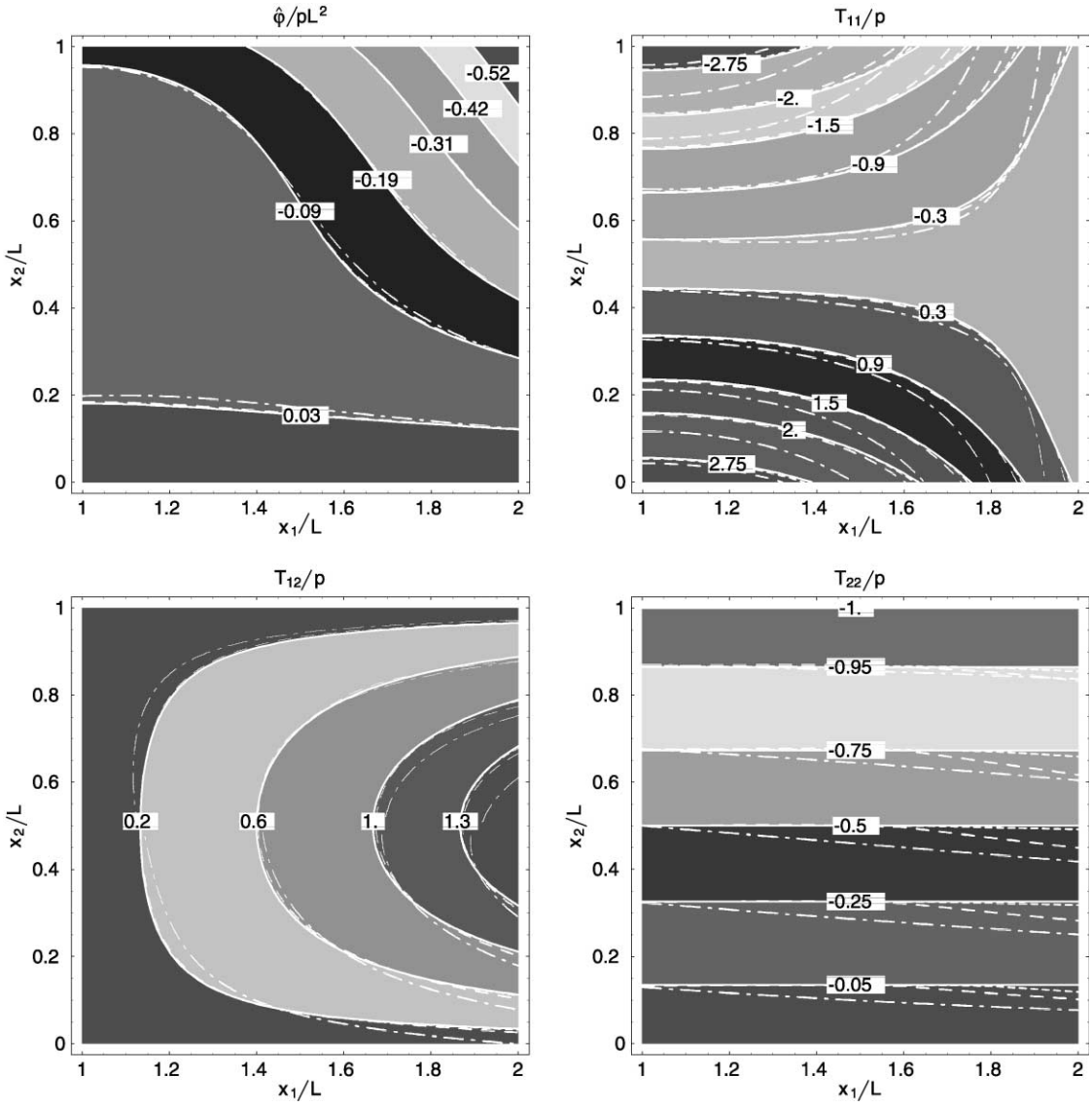

Fig. 8. Convergence of LSM solutions (SFF) for the Example 1. (– – – –) $h = 0.25L$ (25 DOF); (– – – –) $h = 0.10L$ (121 DOF); (- - - - - - -) $h = 0.05L$ (441 DOF); (—) exact solution.

the approximating functions $\tilde{\varphi}_h$, $\widetilde{T}_{h_{11}}$, $\widetilde{T}_{h_{12}}$, $\widetilde{T}_{h_{22}}$ and the contours of the exact solutions, for three different values of h. Convergence of LSM approximations can be observed. In particular, it is seen that the orientation of the primal mesh influences the quality of the approximation only in the case of coarse meshes.

In Fig. 11 we plotted the correlation between the approximation errors

$$e_{h_1} = \frac{\|\widehat{\varphi}_h - \varphi_0\|_1}{\|\varphi_0\|_{4,\infty}}, \quad e_{h_2} = \frac{\|\mathbf{T}_h\widehat{\varphi}_h - \mathbf{T}_0\|_0}{\|\varphi_0\|_{4,\infty}},$$

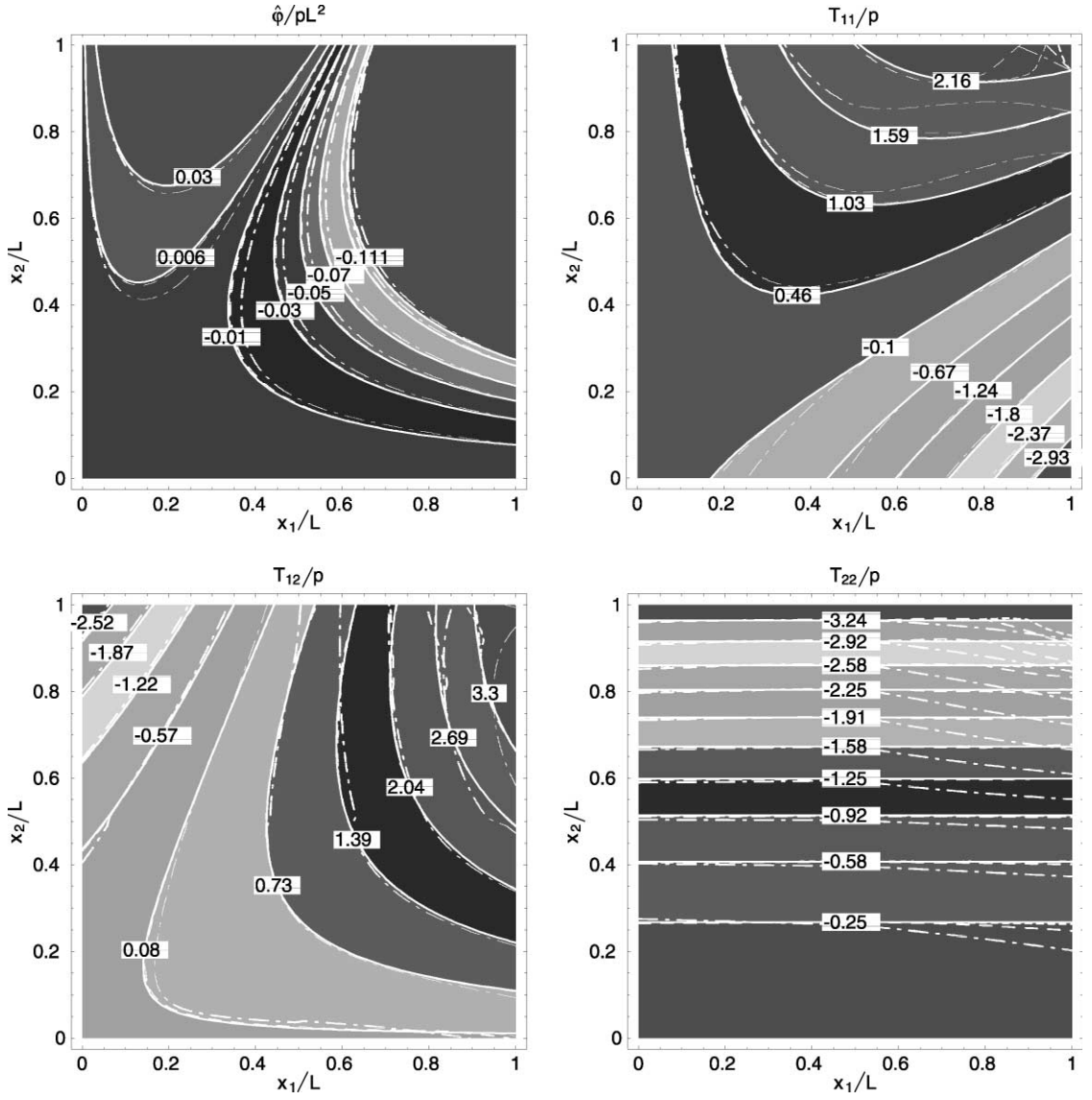

Fig. 9. Convergence of LSM solutions (SFF) for the Example 2. (– – – –) $h = 0.25L$; (– – – –) $h = 0.10L$; $T_{0_{12}} = -\varphi_{0,12} = 0.2327E_1\gamma$; (- - - - - - -) $h = 0.05L$; (—) exact solution.

and the dimensionless mesh size h/H ($H = \sqrt{2}L =$ diameter of the body), $\mathbf{T}_0$ being the stress associated with the exact solution φ_0. We found linear convergence of the stress function (with respect to the $H^1(\Omega)$-norm of φ_0) (Fig. 11(a)). In the first two examples (Fig. 11(b), left), the stress field exhibited the same convergence order (with respect to the $L^2(\Omega)$-norm of $\mathbf{T}_0$). While, in the third example, the convergence order of $\mathbf{T}_h$ was found to be slightly less than one (Fig. 11(b), right). We recorded an approximation error of the stress field in correspondence with the corner nodes of the mesh, which do not satisfy the ($\mathscr{P}_\Sigma$) property discussed in Section 2.3 (Fig. 10, right). This inconvenience can be tackled by extrapolating the stress distribution over the adjacent dual polygons.

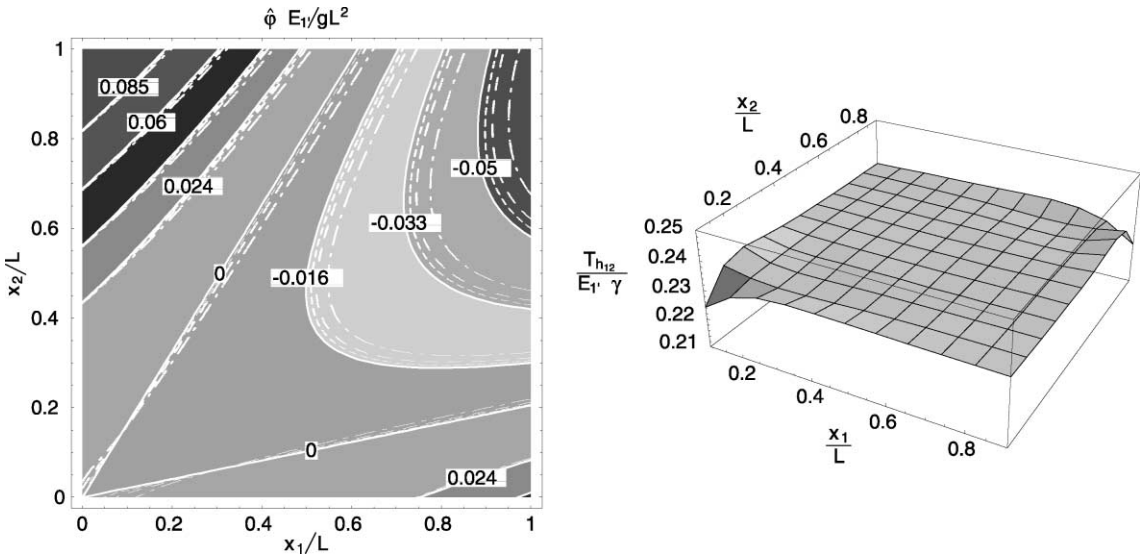

Fig. 10. Convergence of LSM solutions (SFF) for the Example 3 in the terms of the Airy function φ (*left*), and LSM distribution of the stress T_{12} for a 10×10 mesh ($h = 0.10L$ – 121 DOF, *right*). (—) Example 1; (- - - - - - -) Example 2; (– – – –) Example 3.

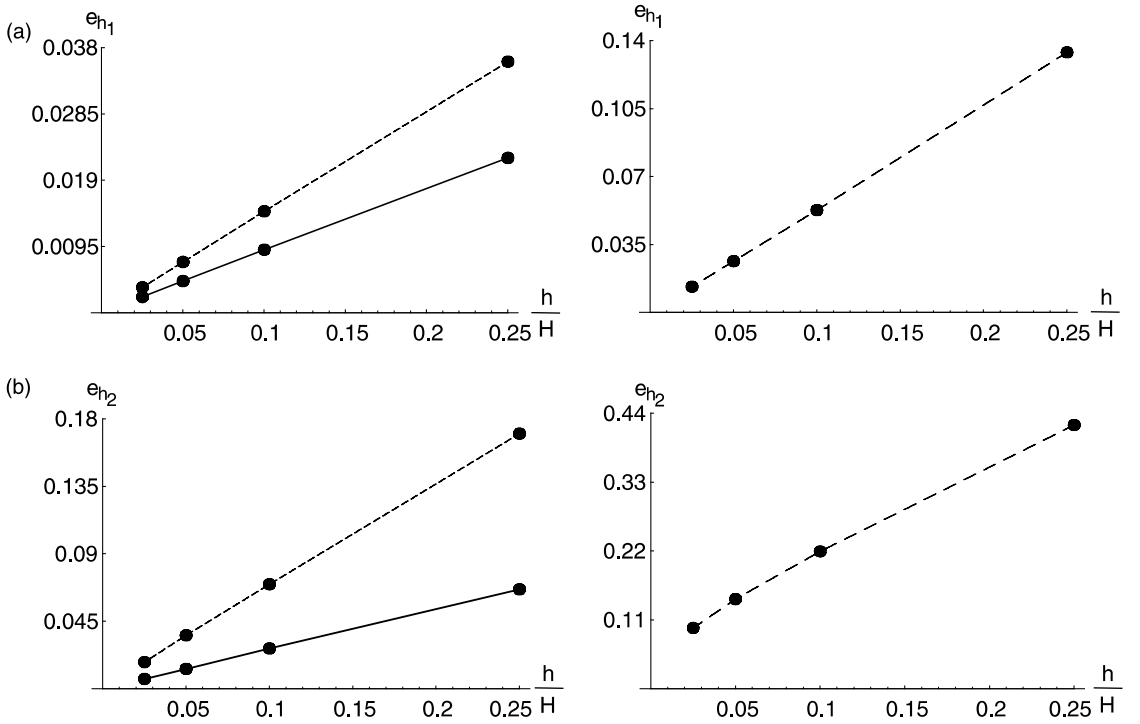

Fig. 11. (a) Plots of the LSM approximation error $e_{h_1} = \|\widehat{\varphi}_h - \varphi_0\|_1 / \|\varphi_0\|_{4,\infty}$ as a function of the mesh size. (—) Example 1; (- - - - - - -) Example 2; (– – – –) Example 3. (b) Plots of the LSM approximation error $e_{h_2} = \|\hat{\mathbf{T}}_h - \mathbf{T}_0\|_0 / \|\varphi_0\|_{4,\infty}$.

6.2. Example 4—Flamant's problem

Fig. 12 illustrates the classical 2D problem of a concentrated vertical load q (per unit thickness) acting on a horizontal straight boundary of an infinitely large plate (*Flamant's problem*). The exact solution of this problem (see, e.g., Fung, 1965) allows for a discontinuity in the slope of the stress function in correspondence with the point-load (Fig. 12, bottom). In polar coordinates (r, ϑ), the only non-zero stress component is T_{rr}, whose contours are circles tangent to the boundary (Fig. 12, top). We reduced the problem to a rectangular domain by applying boundary tractions derived from the exact solution.

The LSM is particularly suitable for Flamant's problem; it can easily reproduce the fold in stress function graph in correspondence with the point-load (Fig. 13). Either successive refinements of a fixed mesh geometry (Fig. 14), and different mesh topologies (Fig. 15) were employed.

6.3. Example 5—Slit-like crack loaded in tension

In order to deepen the particular ability of the LSM in problems with stress singularities, we considered the traction problem of an infinite isotropic plate with a slit-like crack loaded in tension (Fig. 16). We compared the exact solution (cf. Anderson, 1994) with two different LSM approximations and a finite element solution. The latter was obtained through SAP2000®, employing a 15×15 mesh of shell elements

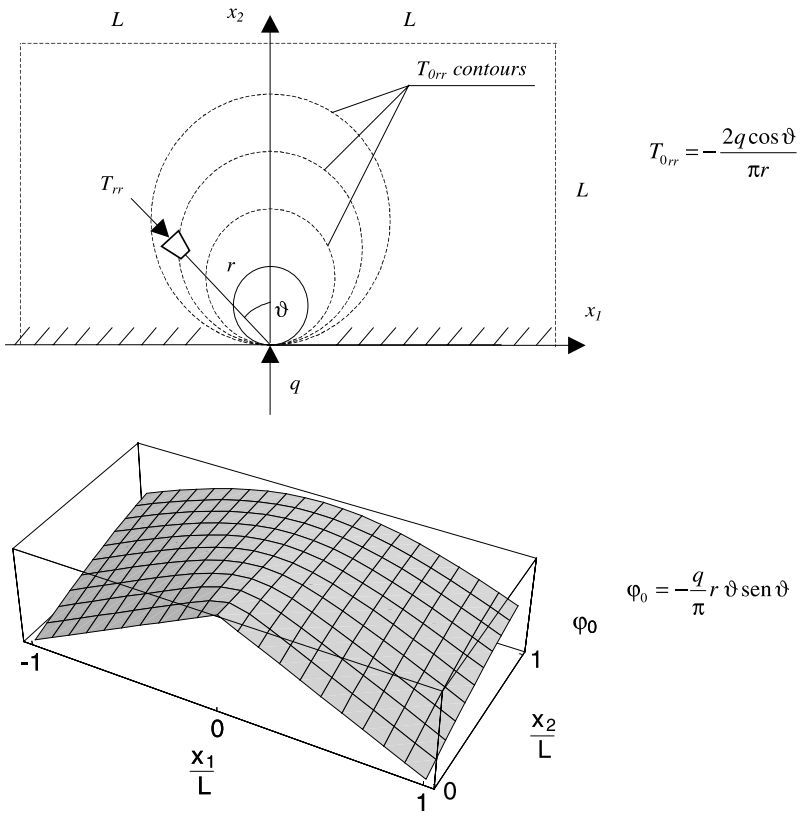

Fig. 12. Flamant's problem—Exact solutions for the radial stress and the stress function.

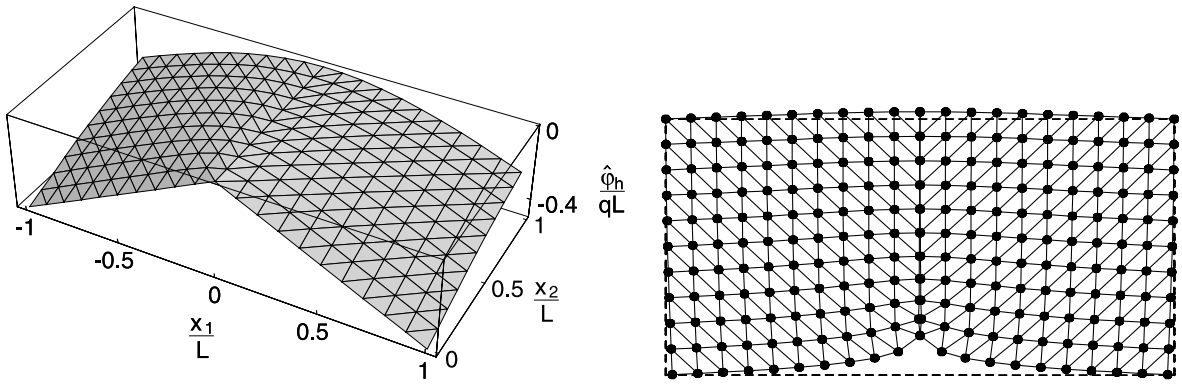

Fig. 13. Polyhedral stress function and deformed shape for the Flamant problem ($h = 0.10L$). (– – – –) $h = 0.25L$; (– – – –) $h = 0.10L$; (- - - - - - -) $h = 0.05L$; (—) exact solution.

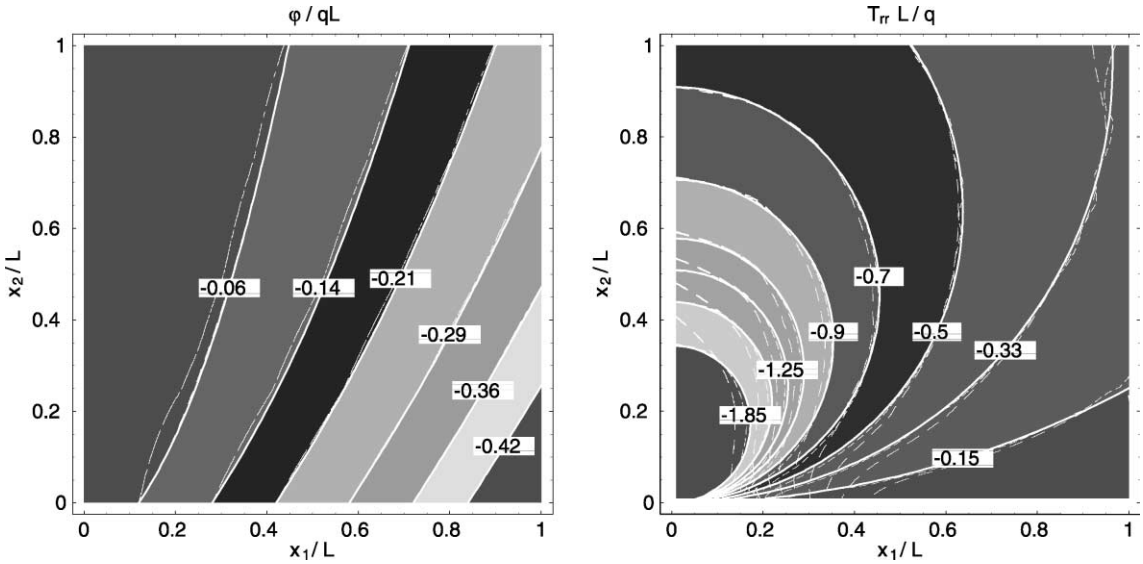

Fig. 14. Convergence of LSM solutions (SFF) for the Flamant problem.

(450 DOF) over a square side 2.5 times larger than the crack length a. As in the previous example, the problem was reduced to a finite domain by applying boundary forces corresponding to the exact solution. Regarding the LSM, two meshes of equal size (441 DOF) and different orientations were employed.

The results in Fig. 16 show that the LSM fits the exact stress distribution near the crack tip better than the examined finite element model, even involving a lower number of degrees of freedom. The discrete force networks corresponding to the LSM approximations are shown in Fig. 17.

6.4. Example 6—A shear wall with openings interacting with a frame

The last problem we dealt with in this work concerns with a structural system formed by a shear wall with openings and a moment resisting frame, subjected to the combined action of vertical and

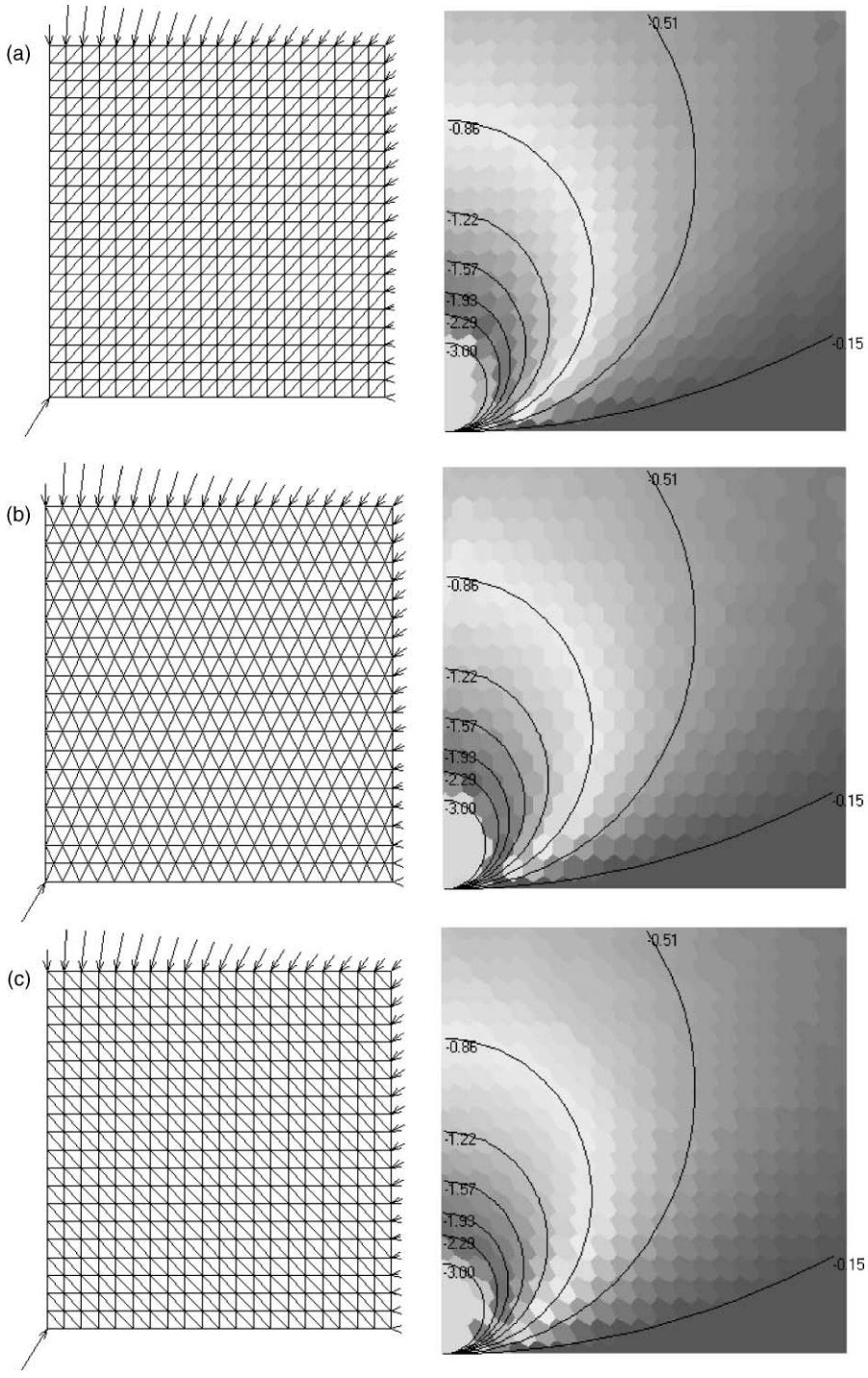

Fig. 15. (a)–(c) Piecewise constant approximation of the radial stress $T_{rr}L/q$ for the Flamant problem and three different LSM meshes ((—) exact contours).

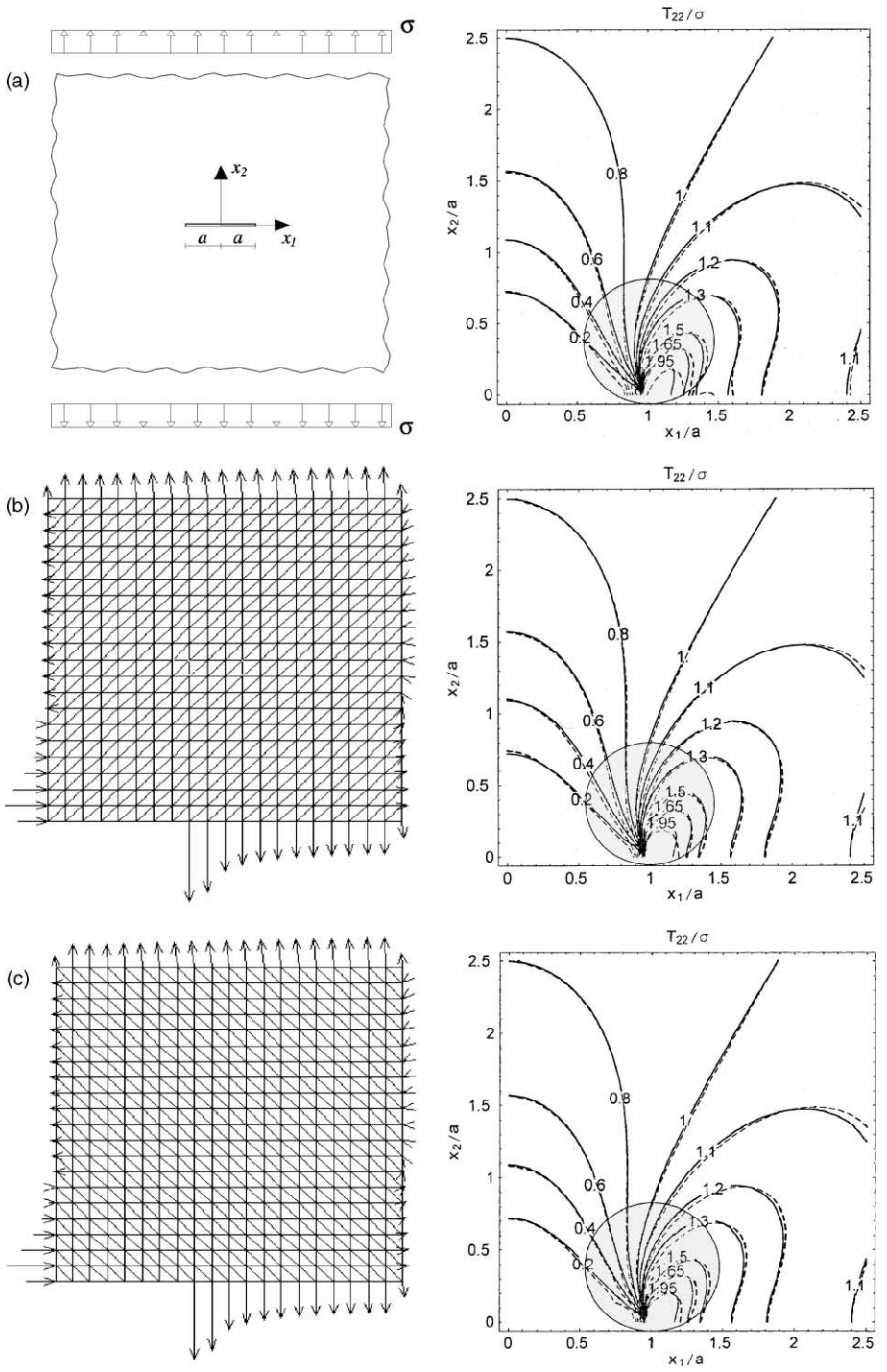

Fig. 16. (a)–(c) Stress concentration around a slit-like crack loaded in tension—Contours of the normal stress T_{22}/σ for a finite element solution (15×15 mesh, 450 DOF, *top*) and two LSM solutions (SFF, 441 DOF, *middle and bottom*).

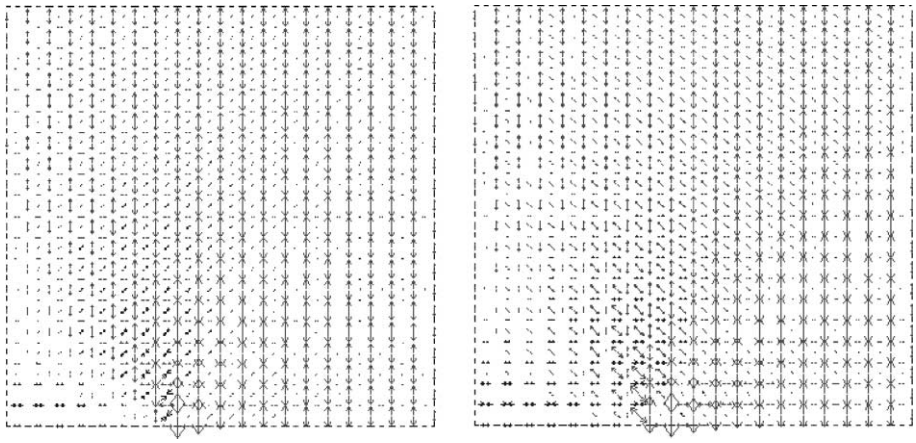

Fig. 17. LSM force networks for a slit-like crack loaded in tension and two different meshes.

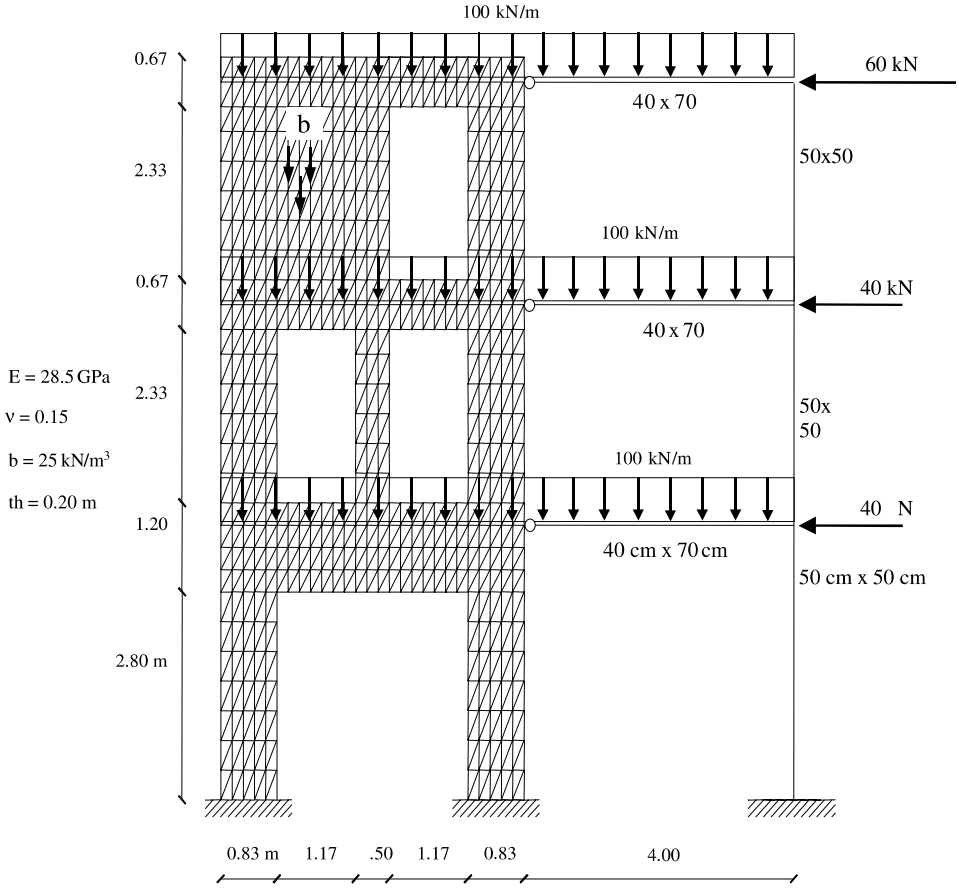

Fig. 18. Shear wall with openings interacting with a moment resisting frame.

horizontal loads (Fig. 18). Material properties of reinforced concrete and hinged connections were considered.

Such a system exhibits a complex mechanical behavior, which is characterized by the effects of stress concentration nearby the connections points and the sharp edges of the wall. The LSM describes the entire system by a collection of 1D elements and allows the user to obtain stress resultants and moments over any structural section of the wall. Indeed, such quantities can be easily computed by summing the contributions due to the axial forces which are intercepted by the generic section.

We analyzed the problem with the NDF of the LSM referring to the primal mesh shown in Fig. 18. We also computed a FEM approximation (SAP2000, 1997), using a mesh of shell elements with the same number of nodes.

Fig. 19 shows the deformed configuration and the force network of the wall given by the LSM. Fig. 20 instead shows the maps of the Cartesian stress components corresponding to both LSM and FEM solutions. Finally, Fig. 21 shows the normal forces, shear forces and bending moments post-computed from the LSM force network in correspondence with several significant sections of the wall, such as the ending sections of the coupling beams and the wall "legs". The LSM ensures that these quantities are balanced with the external loads. Concerning the results in Fig. 20, we can notice a general agreement between LSM and FEM provisions for the stress field, with only small differences essentially at singular points of the wall boundary. In terms of nodal displacements, we recorded a maximum gap of the order of 3% between LSM and FEM results.

7. Closure

In this work we have presented and numerically tested a new method for approximating plane elastic problems, which we refer to as the LSM. Analysis is focused on small deformations of plane continua composed of a generally anisotropic material.

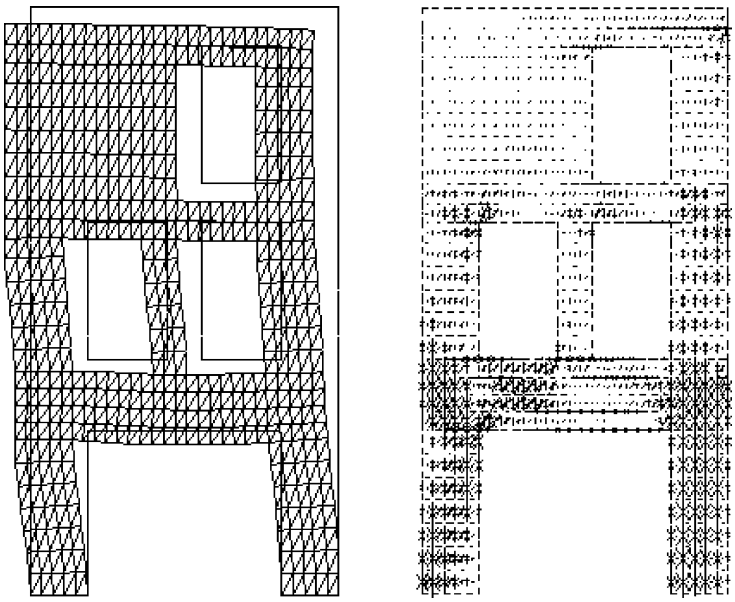

Fig. 19. LSM deformed shape and force network for the wall (NDF).

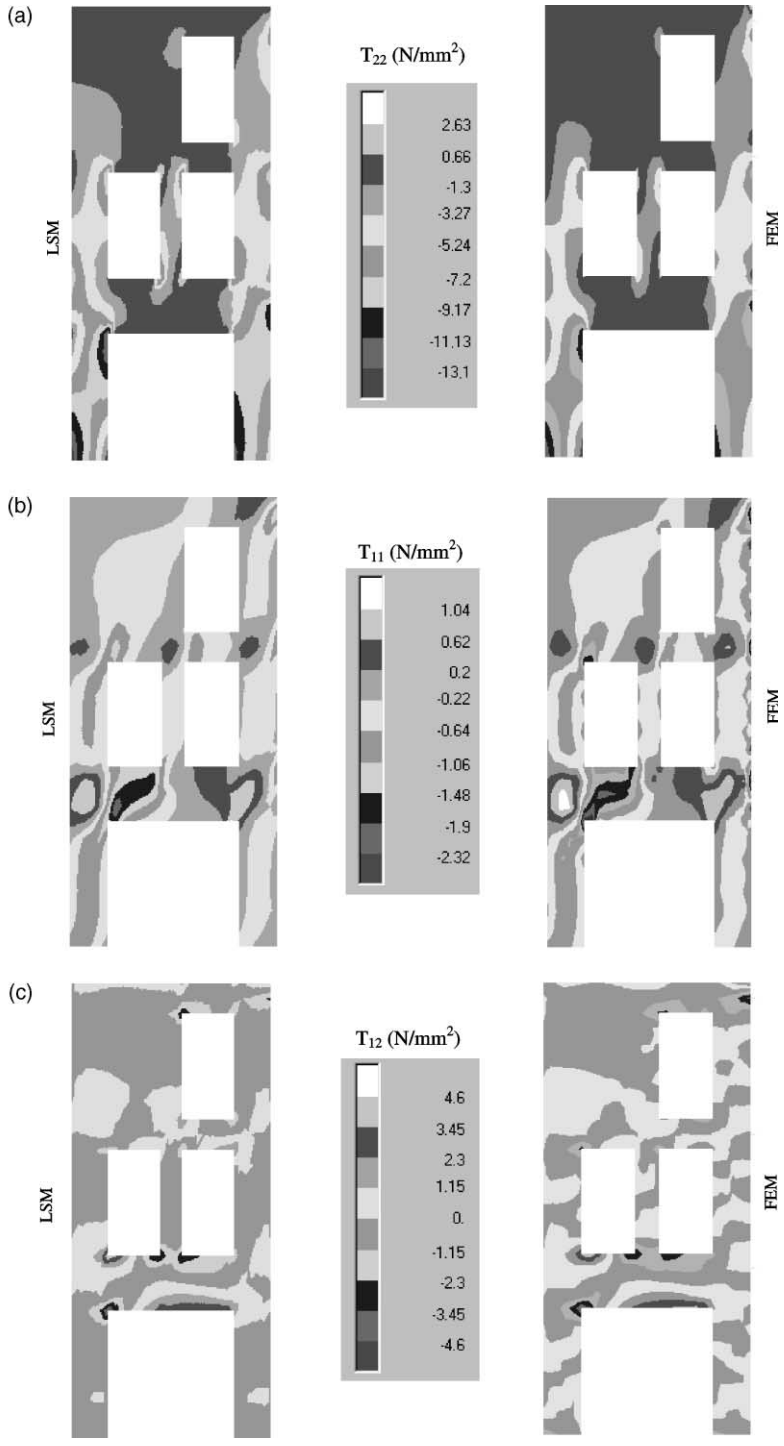

Fig. 20. (a) LSM (NDF) and FEM maps of the stress component T_{22} within the wall for an equal number of nodes. (b, c) LSM (NDF) and FEM maps of the stress components T_{11} and T_{12} within the wall for an equal number of nodes.

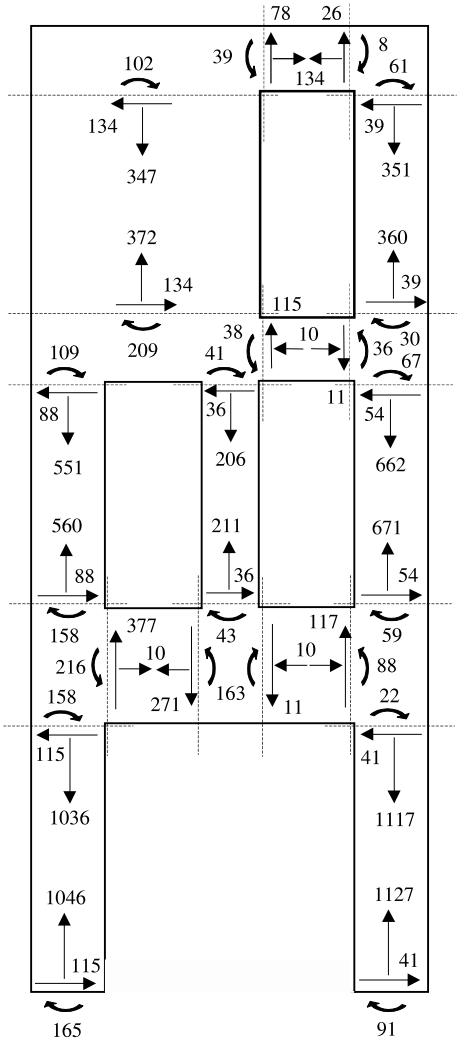

Fig. 21. Axial forces (kN), shear forces (kN) and bending moments (kNm) post-computed from the LSM force network over selected structural sections of the walls.

A crucial feature of this new numerical approach is that it represents an unconstrained, stress based, variational approximation of the boundary value problem.

The LSM, although conceptually more complex than traditional finite element schemes, is easy to implement, and its SFF requires only one degree of freedom per node. The accuracy of the method has been illustrated in several examples.

The LSM also has another appeal: it furnishes a rational way to approximate a continuous body with a latticed structure, thus resolving a familiar problem for structural designers. Due to the form of the constitutive relations, such a truss structure is not conventional.

Its advantages over other traditional approximation techniques, such as the finite element method, are several. In particular:

(a) since singularities are latent in the approximation, the LSM is well suited to treat equilibrium problems with discontinuities and singularities in the geometry or in the data, such as those arising in crack problems and in composite structures;
(b) due to the modeling of a continuum by a latticed structure, the method naturally allows for describing elastic structures composed of both two dimensional and one dimensional elements;
(c) the LSM yields statically admissible stresses and stress resultants at any stage of mesh refinement, as opposed to displacements-based approximation methods;
(d) computation of the compliance (or stiffness) matrix does not require numerical integration.

Nevertheless, in order to maintain the physical significance of the method, it is not possible to enlarge the approximation space of the stress function to include polynomials of order greater than one. Furthermore, in the NDF the stiffness matrix is generally dense.

The present work is open to significant developments such as:

(i) enlargement of the numerical testing by adopting different mesh topologies;
(ii) extension to 3D problems;
(iii) application to boundary value problems with constraints on the stress field, such as problems involving no-tension and elastic–plastic materials;
(iv) development of a mixed approach to the discrete problem to combine the stress function with the NDFs;
(v) inclusion in the LSM of a procedure for the optimization of topology and geometry of the mesh, especially in presence of stress constraints;
(vi) implementation of a convex hull technique to approximate the stress function of a no-tension (or *masonry-like*) body by a concave polyhedra (cf. Giaquinta and Giusti, 1985; Angelillo and Rosso, 1995; Avis and Fukuda, 1992).

Acknowledgements

We wish to express our thanks to Prof. Vittorio Coti Zelati from the Department of Mathematics "Renato Cacciopoli" of the University of Naples for his very helpful assistance with the mathematical aspects of the present work.

References

Absi, E., 1978. Calcul Numérique en Elasticité. Eyrolles, Paris.
Adams, R.A., 1975. Sobolev Spaces. Academic Press.
Alshegeir, A., Ramirez, J., 1992. Computer graphics in detailing strut-tie models. ASCE J. Comput. Civil Eng. 6, 404–416.
Anderson, T.L., 1994. Fracture mechanics: fundamentals and applications. CRC Press.
Angelillo, M., Rosso, F., 1995. On statically admissible stress fields for a plane masonry-like structure. Quart. Appl. Math. 53, 731–751.
Avis, D., Fukuda, K., 1992. A pivoting algorithm for convex hulls and vertex enumeration of arrangements and polyhedra. Discrete Comput. Geom. 8, 295–313.
Balasundaram, S., Bhattacharyya, P.K., 1986. A mixed finite element method for fourth-order partial differential equations. ZAMM–Z. Angew. Math. Mech. 66, 489–499.
Bendsøe, M.P., Kikuchi, N., 1998. Generating optimal topologies in structural design using homogeneization method. Comput. Meth. Appl. Mech. Engng. 71, 197–224.
Biondini, F., Bontempi, F., Malerba, P.G., 1999. Optimal strut-and-tie models in reinforced concrete structures. CAMES 6, 279–293.

Brezzi, F., Fortin, M., 1991. Mixed and Hybrid Finite Element Methods. Springer-Verlag, New York.
Bulman, S., Scienz, J., Hinton, E., 2001. Comparisons between algorithms for structural topology optimization using a series of benchmark studies. Comput. Struct. 79, 1203–1218.
Campbell, S.L., Meyer, C.D., 1991. Generalized Inverses of Linear Transformations. Dover.
Ciarlet, P.G., Raviart, P.A., 1974. A mixed finite element method for the biharmonic equation. In: de Boor, C. (Ed.), Mathematical Aspects of Finite Elements in Partial Differential Equations. Academic Press, pp. 125–145.
Ciarlet, P.G., 1978. The Finite Element Method for Elliptic Problems. North-Holland.
Davini, C., Pitacco, I., 1998. Relaxed notions of curvature and a lumped strain method for elastic plates. SIAM J. Numer. Anal. 35, 677–691.
Davini, C., Pitacco, I., 2000. An unconstrained mixed method for the biharmonic problem. SIAM J. Numer. Anal. 38, 820–836.
Fraternali, F., 2001. Error estimates for a lumped stress method for plane elastic problems. Reports of the Department of Civil Engineering, University of Salerno, 79.
Fung, Y.C., 1965. Foundations of Solids Mechanics. Prentice-Hall.
Giaquinta, M., Giusti, G., 1985. Researches on the equilibrium of masonry structures. Arch. Rational Mech. Anal. 88, 359–392.
Glowinski, R., 1973. Approximations externes, par éléments finis de Lagrange d'ordre un en deux, du problème de Dirichelet pour l'opérateur biharmonique—Méthodes itératives de résolution des problèmes approchés. In: Miller, J.J.H. (Ed.), Topics in Numerical Analysis. Academic Press, pp. 123–171.
Gurtin, M.E., 1972. The linear theory of elasticity. In: Flügge, S. (Ed.), Encyclopedia of Physics, vol. VIa/2. Springer-Verlag.
Hajela, P., Lee, E., 1995. Generic algorithms in truss topological optimization. Int. J. Solids Struct. 32, 3341–3357.
Lions, J.L., Magenes, E., 1968. Problémes aux limites non homogenés et applications, vol. I. Dunod, Paris.
Mish, K.D., 1994. Strut-and-tie modeling of reinforced concrete: a case study in interactive visualization. Proceedings of the National Science Foundation Workshop on Visualization in Earthquake Engineering, Chico, California.
Moreau, G., 1998. Continuum modeling of lattice structures in large displacement applications to buckling analysis. Comput. Struct. 68, 181–189.
Oden, J.T., Carey, G.F., 1983a. Finite Elements–Vol. II: A Second Course. Prentice-Hall.
Oden, J.T., Carey, G.F., 1983b. Finite Elements–Vol. IV: Mathematical Aspects. Prentice-Hall.
O'Dwyer, D., 1999. Funicular analysis of masonry vaults. Comput. Struct. 73, 187–197.
Ohsaki, M., 1998. Simultaneous optimization of topology and geometry of a regular plane truss. Comput. Struct. 66, 69–77.
Papadopoulos, P.G., 1984. A simple algorithm for the linear dynamic analysis of networks. Comput. Struct. 18, 1–8.
Rocchetta, G., 2000. Un moderno software interattivo per la risoluzione dei problemi elastici piani. Thesis, Università degli Studi di Salerno, Salerno, Italy.
SAP2000, 1997. Integrated Finite Element Analysis and Design of Structures. Computers and Structures Inc., Berkeley, California.
Schlaich, J., Schäfer, K., 1991. Design and detailing of structural concrete using strut-and-tie models. Struct. Eng. 69, 113–125.
Scholtz, R., 1978. A mixed method for 4th order problems using linear finite elements. RAIRO Anal. Numérique 12, 85–90.
Scholtz, R., 1979. Interior estimates for a mixed finite element method. Numer. Funct. Anal. Optimiz. 1, 415–429.
Wolfram, S., 1991. Mathematica—A System for Doing Mathematics by Computer, second ed. Addison-Wesley.